KANSAS GEOLOGICAL SURVEY
OPEN-FILE REPORT 93-29

CONCEPTUAL SIMULATIONS OF SALTWATER UPCONING WITH THE USGS SUTRA MODEL

by

Marios Sophocleous
Chong Chung

Disclaimer

The Kansas Geological Survey does not guarantee this document to be free from errors or inaccuracies and disclaims any responsibility or liability for interpretations based on data used in the production of this document or decisions based thereon. This report is intended to make results of research available at the earliest possible date, but is not intended to constitute final or formal publications.

Kansas Geological Survey
1930 Constant Avenue
University of Kansas
Lawrence, KS 66047-3726

Kansas Geological Survey

Conceptual Simulations of Saltwater Upconing with the USGS SUTRA Model

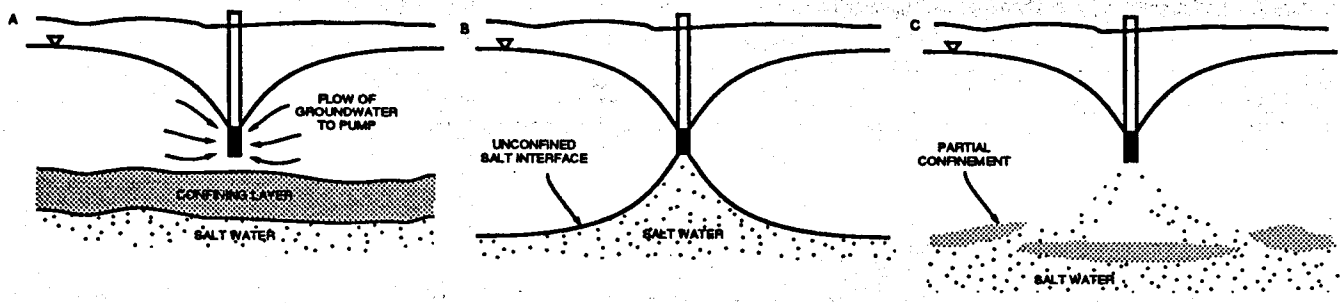

Marios Sophocleous
and Chong Chung

Open-File Report 93-29

GEOHYDROLOGY

The University of Kansas, Lawrence, KS 66047 Tel. (913) 864-3965

Conceptual Simulations of Saltwater Upconing with the USGS SUTRA Model

by
Marios Sophocleous and Chong Chung

Kansas Geological Survey Open-File Report 93-29
September 1993

Executive Summary

In this report we investigate the behavior of brine upconing into a freshwater aquifer under a pumping stress. We developed a conceptual model of the Great Bend Prairie freshwater aquifer overlying the Permian brine-saturated formations; this model is based on the Siefkes site, which has been drilled down to Permian red beds, west of the Big Salt Marsh of the Quivira National Wildlife Refuge in Stafford County, Kansas. We then put this conceptual model into a form suitable for modeling by employing the two-dimensional density-dependent fluid flow and transport numerical code SUTRA, suitably modified and verified for this purpose. Using this model we investigated 11 conceptual model cases to analyze the impact of well pumping on the position of the saltwater-freshwater interface. These cases included realistic uniform and layered aquifer simulations with and without a continuous or discontinuous clay layer. The results are

displayed in numerous figures (the report includes more than 210 graphs) from which the following main conclusions are derived. Extended period pumping, even at reduced rates, still causes saltwater upconing in the absence of recharge. Continuous clay layers above the saltwater-freshwater interface reduce the severity of brine intrusion, depending on how low the clay permeability is. The tighter the clay (i.e., the lower its permeability), the more protection it provides against brine upconing. Even tight clays are ineffective inhibitors of brine intrusion if they contain discontinuities. Low-permeability units generally reduce ground-water flow field intensity, restricting it predominantly to the higher permeability pathways.

Purpose

The purpose of this investigation is to understand how and under what conditions the underlying brine intrudes into the overlying freshwater aquifer, especially under the effect of pumping wells. The case in point is the Great Bend Prairie Cenozoic alluvial aquifer of south-central Kansas, which is underlain by brine-saturated Permian deposits.

Conceptual model

The Siefkes site, located approximately 3 miles west of the Big Salt Marsh of the Quivira National Wildlife Refuge, in T 21 S., R. 12 W. (fig. A), is used as the basis for developing an idealized conceptual model of saltwater intrusion into the overlying freshwater aquifer. Our conceptual model of the site is based on a borehole drilled into the Permian strata. A driller's and geophysical logs of this well are shown in fig. B. Depth to Permian bedrock is approximately 60 m in that area. The location of the saltwater-freshwater interface is approximately at the bedrock contact and is fairly sharp (well defined). The Permian brine has a salinity equal to approximately that of seawater. The depth to the water table (thickness of the unsaturated zone) is approximately 6 m. The aquifer is a typical sand and gravel alluvial deposit with interspersed, relatively thin (1–3 m) clay layers or lenses. A clay layer also exists just above the saltwater-freshwater interface at the Siefkes site. An irrigation well pumping approximately 50×10^{-3}

m^3/s (800 gpm) exists at the site and is screened between 18 and 24 m and between 27 and 37 m. At the scale of several hundred meters to a few kilometers, the aquifer is considered isotropic, layer homogeneous, and unconfined.

Governing equations and computer code

There are two conceptual views of groundwater systems: the aquifer viewpoint and the flow system viewpoint (Anderson and Woessner, 1992). The aquifer viewpoint is used to simulate two-dimensional horizontal flow in confined and unconfined aquifers. The aquifer viewpoint is especially suited to analysis of flow to pumping wells and is the basis for many analytical solutions, including the Theis equation. In this viewpoint, groundwater flow is assumed to be strictly horizontal through aquifers and strictly vertical through confining layers. A general form of the governing equation for the aquifer viewpoint (in the absence of leakage through a confining bed) is

$$\frac{\partial}{\partial x}\left(T_x \frac{\partial h}{\partial x}\right)+\frac{\partial}{\partial y}\left(T_y \frac{\partial h}{\partial y}\right)=S\frac{\partial h}{\partial t}-R, \tag{1}$$

where the terms on the left-hand side of Eq. (1) represent horizontal flow through the aquifer, h is the hydraulic head, T_x and T_y are the components of aquifer transmissivity in the x and y directions, respectively, S is the aquifer storativity, and R is a sink-source term that is defined to be positive for recharge and negative for water withdrawal rate.

In the flow system viewpoint, one is not concerned with identifying aquifers and confining layers per se but with constructing the three-dimensional distribution of hydraulic head and hydraulic conductivities and storativities everywhere in the system. The flow system viewpoint allows for both vertical and horizontal components of flow throughout the system and thereby allows treatment of flow in a two-dimensional profile or in three dimensions. A general form of the governing equation is

$$\frac{\partial}{\partial x}\left(K_x \frac{\partial h}{\partial x}\right)+\frac{\partial}{\partial y}\left(K_y \frac{\partial h}{\partial y}\right)+\frac{\partial}{\partial z}\left(K_z \frac{\partial h}{\partial z}\right)=S_s\frac{\partial h}{\partial t}-R^*, \tag{2}$$

where K_x, K_y, and K_z are components of the hydraulic conductivity in the three cartesian coordinates x, y, and z, respectively, S_s is specific storativity, and R^* is a general sink-source term defining the volume of inflow to the system per unit volume of aquifer per unit of time (negative for outflow).

Cross-sectional or profile models are useful when vertical flow is important, but a full three-dimensional model is unwarranted. A profile model assumes that all flow occurs parallel to and in the plane of the profile. In other words, there is no component of flow at an angle to the profile. For this reason, standard profile models are not useful in simulating point sources or sinks of water, such as wells embedded in the profile because they create radial flow. Axisymmetric profile models, however, can be used to simulate the effects of pumping wells. Axisymmetric models are cross-sectional models with radial-cylindrical coordinates (r, z) and therefore can accommodate point sources and sinks within the profile where the source or sink is located at $r = 0$. Standard profile models can be tricked into simulating axisymmetric profiles by adjusting the thickness of the profile and the grid-cell-assigned transmissivity and storativity.

SUTRA (Voss, 1984) is a two-dimensional hybrid finite-element and integrated finite-difference numerical method for simulating density-dependent fluid flow and transport of either a single-species solute or energy in a saturated aquifer or unsaturated deposits. SUTRA simulates areal and cross-sectional flow. The model coordinate system can be an areal plane, cross-sectional Cartesian (x, y) coordinates, or cross-sectional radial-cylindrical (r, z) (axisymmetric) coordinates. Because of these attractive features, we employed the SUTRA model to simulate saltwater upconing around irrigation wells in the Great Bend Prairie aquifer of south-central Kansas. The two-dimensional fluid-density-dependent ground-water flow equation of the SUTRA model takes the form

$$\rho S_{sp} \frac{\partial p}{\partial t} + \phi \frac{\partial \rho}{\partial C} \frac{\partial C}{\partial t} + \nabla \cdot (\phi \rho \mathbf{v}) = Q_p, \tag{3}$$

where: ρ is the fluid density [M/L^3], S_{sp} is the specific pressure storativity [M/(LT^2)]$^{-1}$ =

$(1-\phi)\,\alpha + \phi\beta$ (S_{sp} is related to specific storativity S_s [L^{-1}] by $S_S = \rho|g|S_{sp}$, where |g| [L/T^2] is the magnitude of the gravitational accerleration); α is the matrix compressibility [$(M/LT^2)^{-1}$]; β is the fluid compressibility [$M/(LT^2)$]$^{-1}$; p is the fluid pressure [M/LT^2; (N/m^2 or Pa)]; C is the salt concentration as a mass fraction (mass solute/mass fluid); **v** is the fluid velocity vector [L/T]; and Q_p is the fluid mass source (mass fluid/aquifer volume/time) [M/L^3T]. The symbol ∇ (del) is the vector differential operator representing the three-dimensional gradient in space.

The salt-transport equation of the SUTRA model is

$$\phi\rho\frac{\partial C}{\partial t} + \phi\rho\mathbf{v}\cdot\nabla C - \nabla\cdot\left[\phi\rho(D_m I + D)\cdot\nabla C\right] = Q_p\left(C^* - C\right), \tag{4}$$

where D_m is the molecular diffusion coefficient of salt [L^2/T]; I is the identity tensor; D is the mechanical dispersion tensor [L^2/T]; and C^* is the salt concentration as a mass fraction in the source fluid.

These equations are coupled in the following ways. First, the fluid velocity in Eq. (3) is calculated according to Darcy's law:

$$\mathbf{v} = -\left(\frac{k}{\phi\mu}\right)\cdot(\nabla p - \rho\mathbf{g}), \tag{5}$$

where k is the permeability tensor [L^2]; μ is the fluid dynamic viscosity [M/LT^2]; and **g** is the gravity vector [L/T^2]. The hydraulic conductivity K [L/T] can be identified as $K = \rho g k/\mu$. Second, the density dependence on salinity (concentration) is a linear function:

$$\rho = \rho_O + \frac{\partial\rho}{\partial C}(C - C_o), \tag{6}$$

where ρ_O is the fluid density when $C = C_O$; C_O is a base salt concentration; and $\partial\rho/\partial C$ is a constant coefficient of density variability.

Code modifications

A number of modifications to the SUTRA code were done to ease data processing and analysis. Only two modifications that have an impact on model simulations or data display and analysis are presented here. The first and main modification is related to aquifer specific

storativity, specifically, to porous matrix compressibility α. The SUTRA codes provides for spatially variable permeability and longitudinal and transverse dispersivities and for variable porosity, thickness, and hydraulic head values. However, it does not provide for spatially variable matrix compressibility and hence specific storativity. This is important in our case because we want to simulate a layered system such as a Cenozoic alluvial aquifer overlying a Permian aquifer of different permeability and storativity. Therefore the code is modified to read a spatially variable matrix compressibility for each node in the grid characterizing a cell area around each node.

The second modification is the creation of a SUTRA postprocessor for calculating hydraulic head values based on the model-estimated nodel fluid pressure and density values and on the position (elevation) of each node ($h = p/(\rho g) + z$). In addition, our SUTRA postprocessor converts the SUTRA output to a form suitable for input to the powerful TECPLOT program for displaying contours of concentration, pressure, hydraulic head, and flow velocity vectors.

We also enhanced the SUTRA preprocessing module by adding an irregular grid mesh generator and by generating a hydrostatic pressure distribution based on a fluid concentration-depth distribution for initial conditions and specified pressure boundary condition specifications.

Code verification

Code verification refers to comparison of the numerical solution generated by the model with one or more analytical solutions or with other numerical solutions. In addition to a number of verification runs described in the SUTRA manual (Voss, 1984), which we confirmed by rerunning the model, we tested the SUTRA model in both the areal (aquifer viewpoint) and cross-sectional modes against the Theis analytical solution for a pumping well. Table 1 describes one set of such tested cases.

Table 1. Analytical vs. numerical solution test case.

Aquifer areal dimensions: 1600 m × 1600 m; no-flow boundaries
Grid cell dimensions: 40 m × 40 m
Aquifer properties: $K = 1.06 \times 10^{-4}$ *m/s* (30 ft/d); $S = 0.05$; saturated thickness, $b = 160$ m
Initial hydraulic head: 200 m (uniform)
One pumping well: $Q = 58.67 \times 10^{-3}$ m^3/s (930 gpm)
Time step size $\Delta t = 6$ hr; total simulation time = 3 days

The cross-sectional simulations were run in two modes: (1) Using rectangular coordinates (x, y) of constant cell dimensions of 40 m × 40 m and (2) using radial-cylindrical coordinates (r, z) of (a) constant radial cell dimensions of 40 m × 40 m (21 × 5 nodes) and (b) variable radial cell dimensions with rectangular cells increasing in size with distance from the center axis (well at $r = 0$) (93 × 5 nodes). In the vertical direction the nodal spacing is constant (40 m).

Table 2 compares the results of the areal and cross-sectional simulations with those of the Theis analytical solution after 3 days of continuous pumping.

The hydraulic head contours at 3 days since pumping began using our postprocessing programs are shown in fig. 1 together with the employed grid. The resulting profiles of the cone

Table 2. Comparisons of SUTRA-calculated drawdown with analytical solution for test case shown in Table 1.

	Distance from well (m)		
	40	80	200
Analytical drawdown (m) sol'n	1.33	0.95	0.46
Single-layer areal model	1.25	0.93	0.46
Cross-sectional models			
rectangular (unadjusted)	3.16	2.78	1.84
rectangular (adjusted[a])	1.38	1.05	0.41
radial-cylindrical (constant grid)	1.29	0.94	0.46
radial-cylindrical (variable grid)	1.32	0.94	0.46

[a]Profile S adjusted as follows: $S = \frac{Sb}{\Delta y}$.

of depression at 6 hr and 3 days since pumping began are shown in fig. 2. Figures 3 and 4 display the radial-cylindrical profile models of constant and variable radial grid sizes, respectively. In figs. 3 and 4, the pressure (a), hydraulic head (b), and grid mesh (c) are displayed. The results are in satisfactory agreement with the analytical solution; the variable-grid radial-cylindrical profile resulted in a better match with the analytical solution than the other cross-sectional models shown in Table 2.

Model design

The conceptual model described previously based on the Siefkes site is put into a form suitable for modeling. This step includes designing the grid, selecting time steps, setting boundary and initial conditions, and selecting values of aquifer parameters and hydrologic stresses. Based on the results of the above-mentioned code verification step, we adopted the variable-grid radial-cylindrical cross-sectional model design for our conceptual model simulations. Figure 5 displays the grid geometry we adopted. The mesh contains 40 rows of constant spacing of 2 m and 24 columns of elements with expanding width with increasing distance from the well, which is located along the $r = 0$ axis. The first column width is equal to a well radius of 0.4 m. Maximum radial distance from the well is 3,169 m. The number of nodes is 1,025, and the number of elements in the mesh is 960. Table 3 displays the model parameters we selected based on our preliminary knowledge of the study area. The table includes aquifer and fluid properties, other input parameters, and hydrologic stresses and time steps employed. A continuous or discontinuous clay layer of 8 m thickness was also considered. Figure 6 displays the grid with a discontinuous clay layer examined.

Boundary conditions include no flow everywhere except where hydrostatic pressure and concentration are specified at the right-hand side boundary nodes; any water that enters the section through those nodes has freshwater concentration (C_0) above the interface, and brine fluid concentration (C) below it. A well pumping is specified at the left-hand side boundary

Table 3. Model parameters employed in the conceptual Siefkes test case

Parameter	Value
Aquifer, fluid, and other parameters	
hydraulic conductivity	$K = 23$ m/d (75 ft/d)
intrinsic permeability	$k = 2.70 \times 10^{-11}$ m^2
porosity	$\phi = 0.20$
storativity	$S = 0.15$
specific storativity	$S_s = 0.002$ m^{-1}
bulk porous matrix compressibility	$\alpha = 2.58 \times 10^{-7}$ [kg/m s^2)]$^{-1}$
water compressibility	$\beta = 4.40 \times 10^{-10}$ [kg/(m s^2)]$^{-1}$
apparent solute molecular diffusivity	$D_m = 6.6 \times 10^{-6}$ m^2/s
longitudinal dispersivity	α_L =10 m
transverse dispersivity	$\alpha_T = 0.5$ m
base fluid (water) density	$\rho_o = 1{,}000$ kg/m^3
brine density	$\rho = 1{,}025$ kg/m^3
solid grain density	$\rho_s = 2{,}650$ kg/m^3
fluid (water) viscosity	$\mu = 1.0 \times 10^{-3}$ kg/(m s)
base fluid (water) salt concentration	$C_o = 0$
brine fluid salt concentration	$C = 0.035$
density change with concentration	$\partial\rho/\partial C = 700$ kg/m^3
saturated thickness	$b = 74$ m
depth to water table	dtw = 6m
depth to freshwater-saltwater interface	60 m
depth to Permian boundary	60 m
fluid pumping rate	$Q_p = 50$ kg/s (~800 gpm)
gravitational acceleration	$g = 9.81$ m/s^2
initial time step duration	60 s
time step multiplier	1.2
maximum time step size	1 mo
total simulation time	2 yr
Clay layer properties	
thickness	8 m
hydraulic conductivity	0.06 m/d or 1.1 m/d
storativity	0.075
Underlying Permian aquifer properties	
thickness within model section	20 m
hydraulic conductivity	2.3 m/d
storativity	0.075

($r = 0$). The system initially is at hydrostatic pressure with the saltwater-freshwater interface located horizontally at a depth of 60 m, which is 54 m below the water table.

Simulation results and sensitivity analysis

Table 4 presents 11 conceptual modeling cases considered in analyzing the impact of variations in aquifer parameters, geometry, pumping stresses, and boundary conditions on the system with particular emphasis on the location of the freshwater-saltwater interface. The interface is defined here as the 50% concentration contour between fresh water and brine. The results from all cases outlined in table 4 are displayed in sets of six parts (a through f) per case (figs. 7-17) as follows: 1) Sets of concentration contours (a) and interface location (b) displayed at 1.8 weeks (upper) and 6.4 months (lower) since pumping began; magnification insets of concentration contours and interface location near the pumping well are also presented at 6.4 months since pumping began; (2) sets of fluid pressure contours (c) and water table (0 isobar) location (d) displayed at the same times as in item 1; magnification insets of pressure contours and water table near the pumping well are also presented at 6.4 months since pumping began; and (3) sets of hydraulic head contours (e) displayed 1.8 weeks (upper), 6.4 months (middle), and 2.0 years (lower) since pumping began and of flow vectors (f) displayed at 2.0 years since pumping began; a magnification inset of flow vectors near the pumping well at that time is also presented.

All 11 cases are summarized with regard to the effect of pumping on the location of the saltwater-freshwater interface in figures 18–21. Figures 7–21 provide insights into the behavior of saltwater-freshwater interface under a pumping stress, as we will explain below.

With regard to figs. 7–17, we highlight only a few points. The saltwater-freshwater dispersion zone is clearly defined, especially as shown after 1.8 weeks of pumping in figs. 7a–17a (upper figures). The impact of pumping on this dispersion zone is clearly indicated, especially after 6.3 months of pumping in figs. 7a–9a (lower figures). Note that the pumping well screen is located in the depth intervals 18–24 m and 27–37 m, which correspond,

Table 4. Model test cases analyzed in this report.

Case No.	Explanation	Figure
1	Base case: Uniform aquifer system over entire model region (no Permian formation properties distinction, no clay layer); K = 23 m/d (75 ft/d) and S = 0.15. Initial saltwater-freshwater interface at 54 m below water table. Well pumping at 0.05 m^3/s (~ 800 gpm); longitudinal and transverse dispersivities: α_L = 10 m, α_T = 0.5 m	7, 18
2	Same as case 1 but pumping reduced to 0.125m^3/s (~200 gpm).	8, 18
3	Same as case 1 but longitudinal dispersivity reduced to α_L = 1 m.	9, 18
4	Same as case 1 but a continuous clay layer of K = 0.06 m/d (0.2 ft/d), but same storativity as rest of aquifer (S = 0.15), is introduced.	10, 19
5	Same as case 4 but clay storativity reduced to half of that of the rest of the aquifer.	11, 19
6	Same as case 4 but aquifer (and clay) storativity is reduced to S = 0.075.	12, 19
7	Same as case 4 but bottom boundary condition switched to specified brine concentration.	13, 19
8	Same as case 4 but clay is discontinuous (see figure 6).	14, 20
9	Same as case 8 but clay storativity (S = 0.075) reduced to half of that of the rest of the aquifer.	15, 20
10	Same as base case but with lower Permian aquifer characterized by K= 2.3 m/d (7.5 ft/d) and S = 0.075.	16, 21
11	Same as case 10 but with continuous clay layer of K= 1.1 m/d (3.75 ft/d).	17, 21

respectively, to 62–56 m and 53–43 m above the 0 reference level displayed in all figures. The initial saltwater-freshwater interface is thus located 23 m below the bottom of the lower well screen. Therefore, as these figures (as well as the saltwater-freshwater interface indicating figures 7b–9b) indicate, we have saltwater upconing into the pumping well as shown after approximately 6 months of continuous pumping. In the concentration-displaying figures, the lighter the color, the saltier the water. [The salt concentration scale ranges from black for zero salt concentration (fresh water) to white for brine concentration (C = 0.035). Because of the no-flow bottom boundary conditions, the saltwater is progressively getting diluted with time during

pumping.] Also note the scale difference of the insets compared to the much larger radial distance displayed in the lower (a) figures. With regard to the fluid pressure figures 7c–17c, the higher the pressure, the lighter the color; the pressure scale is in Pascals [newtons/m^2 or $kg/(m \cdot sec^2)$].

The impact of "tight" continuous clays is illustrated in figs. 10–13: a dramatic dumping of saltwater upconing. The (b) groups of these figures, especially when compared to the corresponding ones of figs. 7–9, demonstrate this effect clearly. Also note the dramatic impact of tight clay layers on ground-water velocities, shown in the (f) groups of figs. 10–13, especially when compared with the corresponding ones of figs. 7–9. The pumping-induced ground-water flow velocities below the clay layer are practically neutralized (i.e., minimized); the flow field is essentially reduced to the area above the clay layer, and the pronounced vertical gradients in figs. 7f–9f, which are caused by the pumping well screened in the upper part of the aquifer, are significantly reduced in figs. 10f–13f.

The damping effect of similarly tight but discontinuous clays on saltwater upconing is not as pronounced (see figs.14a,b and 15a,b) as the effects seen in figs. 10–13. Note the clay discontinuity (hole) effect on ground-water flow velocities in figs. 14f and 15f

The impact of a low-permeability Permian aquifer and of a clay layer that is not as tight as the one described previously are shown in figs. 16 and 17, respectively. Note the dumping impact of the low-permeability Permian strata on ground-water flow vectors (fig. 16f), especially when compared with the base case (fig. 7f). Also note that the saltwater-freshwater interface (figs. 16b and 17b) is below the bottom well screen.

Finally, the impact of the considered reduced storativities and longitudinal dispersivities, reduced pumpage at the considered time and spatial scales, and specified brine concentrations at the lower model boundary had minor effects on concentration and pressure distributions within the model domain. Additional model runs are required to check the range of impact of these variables on the system. It should be noted that each computer run of the model system

described in table 3 took at least 22 minutes of real time on a 486/50 MHz PC with a Lahey 5.0 compiler.

Our results are summarized and highlighted with respect to the saltwater-freshwater interface behavior after 6.4 months of continuous pumping in figs. 18–21. (The numbers shown at the top headings refer to the test cases in Table 4.) Briefly, with regard to fig. 18, even reducing pumpage (50 kg/s or 800 gpm) by a factor of 4 still has a significant impact on saltwater upconing after 6.4 months of continuous pumping at the scale considered. Changing longitudinal dispersivity from 10 m to 1 m had no impact on the location of the interface. With regard to fig. 19, the effect of a tight (K = 0.06 m/d = 0.2 ft/d) 8-m continuous clay layer just above the saltwater-freshwater interface on interface upconing is dramatic. Reducing the considered clay and or aquifer storativity by half and changing the bottom boundary conditions with respect to concentrations to specified brine concentration had no apparent impact on the location of the interface. With regard to fig. 20, a tight clay seems unable to control the location of the interface if the layer has discontinuities. Finally, with regard to fig. 21, lower permeability layers (1.1 m/d or 3.75 ft/d to 2.3 m/d or 7.5 ft/d) have an appreciable impact on the location of the interface, but not as dramatic as the one exhibited by tight clays (K = 0.06 m/d or 0.2 ft/d) at the spatiotemporal scales considered in this study.

Conclusions

The purpose of this investigation is to use conceptual modeling in a plausible set of scenarios to better understand the behavior of brine upconing into a freshwater aquifer under pumping stress and the principal factors affecting this behavior. Despite the limited range of considered factors in this investigation, the results of this study elucidated a number of interesting points.

1. Extended-period pumping, even at reduced rates, still causes saltwater upconing in the absence of recharge.

2. Continuous clay layers above the saltwater-freshwater interface reduce the severity of brine intrusion depending on how low the clay permeability is. The tighter the clay (i.e., the lower its permeability), the more the protection it provides against brine upconing.
3. Even tight clays are ineffective inhibitors of brine intrusion if they contain discontinuities.
4. Low-permeability units generally reduce ground-water flow field intensity, restricting it predominantly to the higher permeability pathways.
5. Changes in aquifer storativity have only a minor effect on the position and movement of the saltwater-freshwater interface.

Acknowledgments

Bob Buddemeier and Hillel Rubin (visiting scientist at KGS) provided constructive comments on this report.

References

Anderson, M.P., and Woessner, W. W., 1992. Applied Groundwater Modeling—Simulation of Flow and Advective Transport. Academic Press Inc., San Diego, California, 381 p.

Buddemeier, R. W., Garneau, G., Healey, J. M., Ma, T. S., Sophocleous, M. A., Whittemore, D. O., Young, D., and Zehr, D., 1993. The Mineral Intrusion Project: Report of Progress During Fiscal Year 1993, 157 p.

Voss, C. I., 1984. SUTRA: A finite-element simulation model for saturated-unsaturated fluid-density-dependent ground-water flow and energy transport or chemically reactive single-species solute transport. U.S. Geological Survey, Water Resources Investigations Report 84-4369, 409 p.

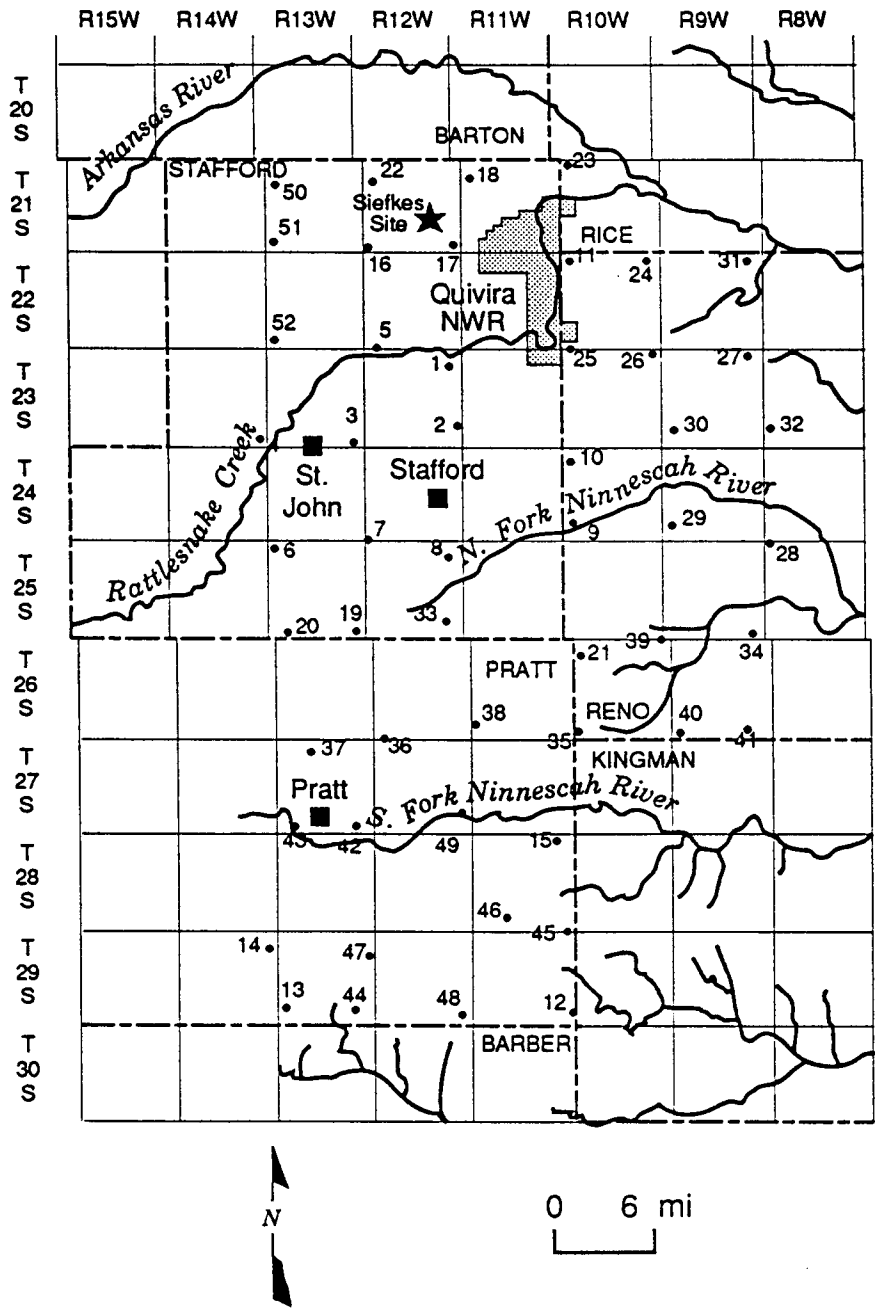

Figure A. Location of Siefkes study site. Observation wells in the KGS/GMD5 monitoring-well network are also indicated.

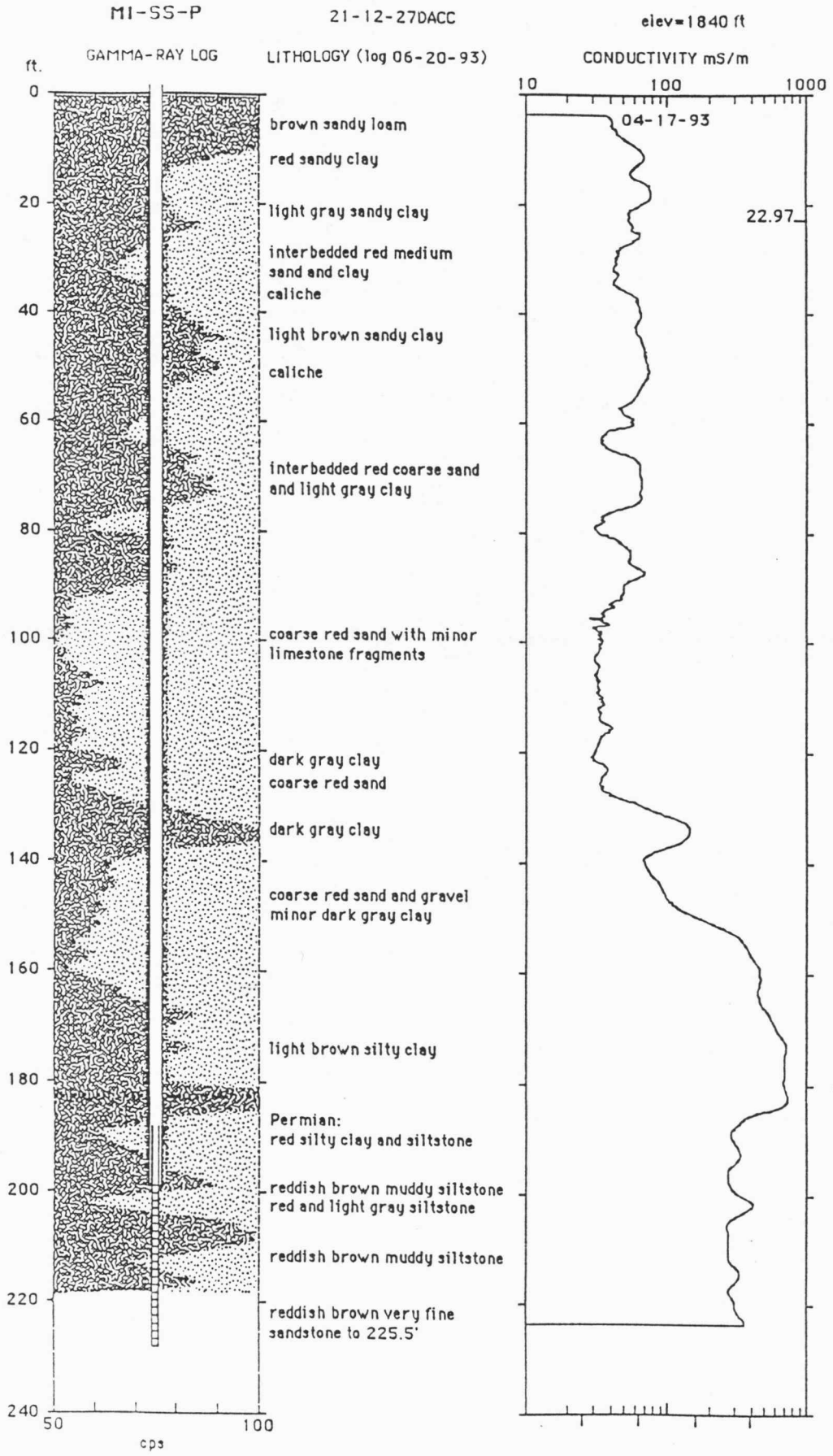

Figure B. Gamma-ray, formation conductivity, and drilling log for the Permian monitoring well at the Siefkes site (Adapted from Buddemeier et al., 1993).

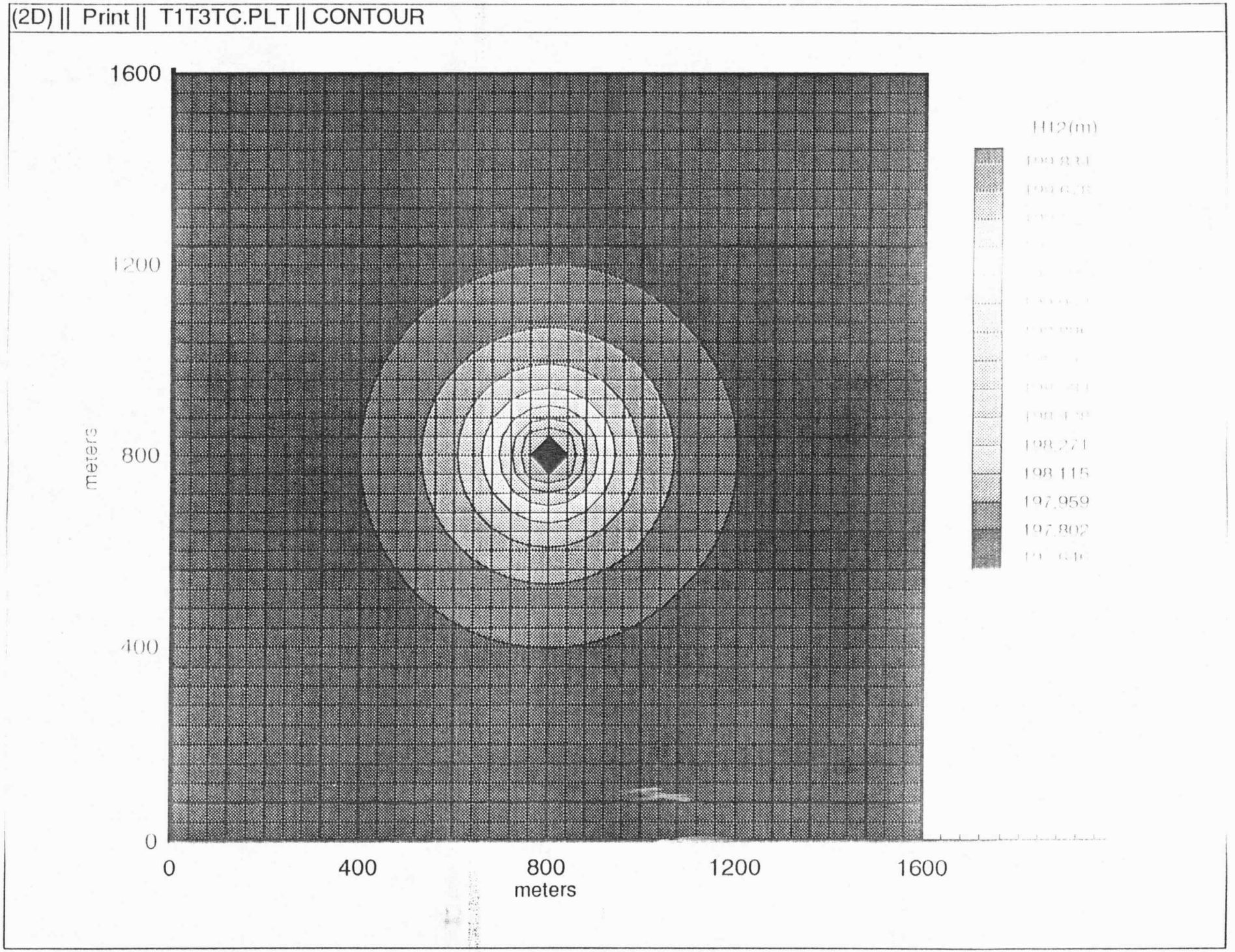
(2D) || Print || T1T3TC.PLT || CONTOUR
1600
1200
800
400
0
meters
0
400
800
1200
1600
meters
1112(m)
198.271
198.115
197.959
197.802

Figure 1

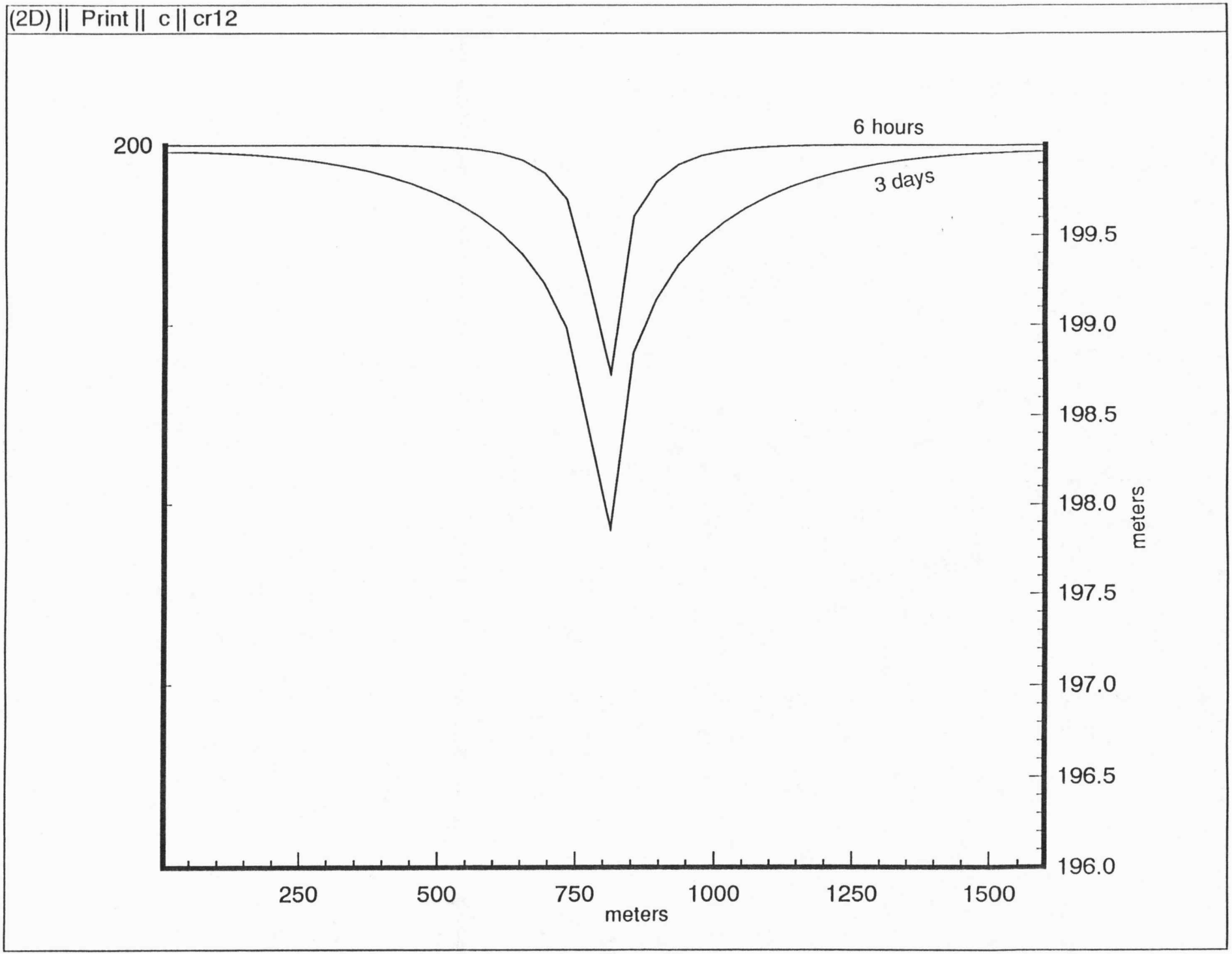
(2D) || Print || c || cr12
6 hours
3 days
200
199.5
199.0
198.5
198.0
197.5
197.0
196.5
196.0
meters
250
500
750
1000
1250
1500
meters

Figure 2

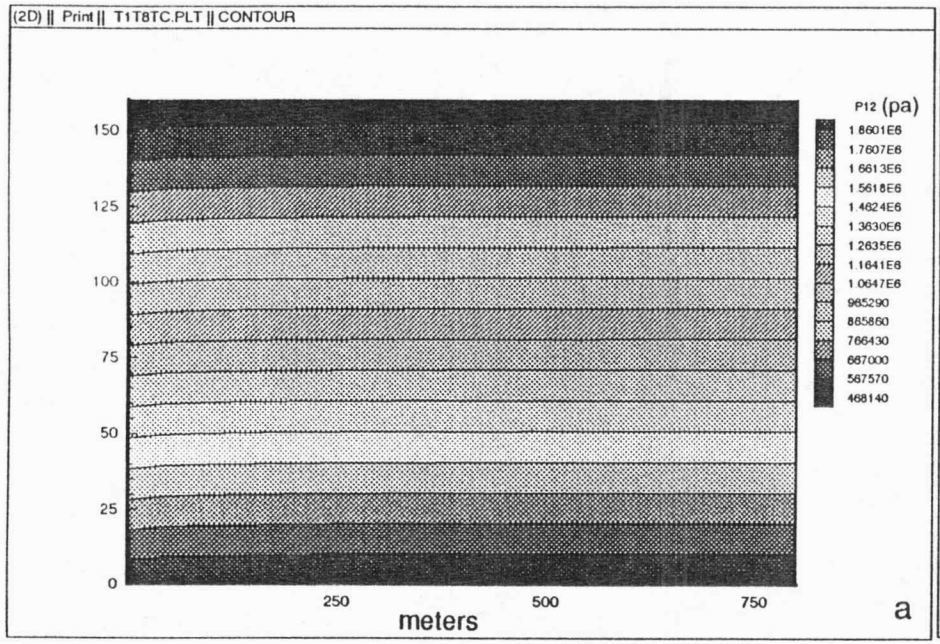
(2D) || Print || T1T8TC.PLT || CONTOUR
P12 (pa)
1.8601E6
1.7607E6
1.6613E6
1.5618E6
1.4624E6
1.3630E6
1.2635E6
1.1641E6
1.0647E6
965290
865860
766430
667000
567570
468140
150
125
100
75
50
25
0
250
500
750
meters
a

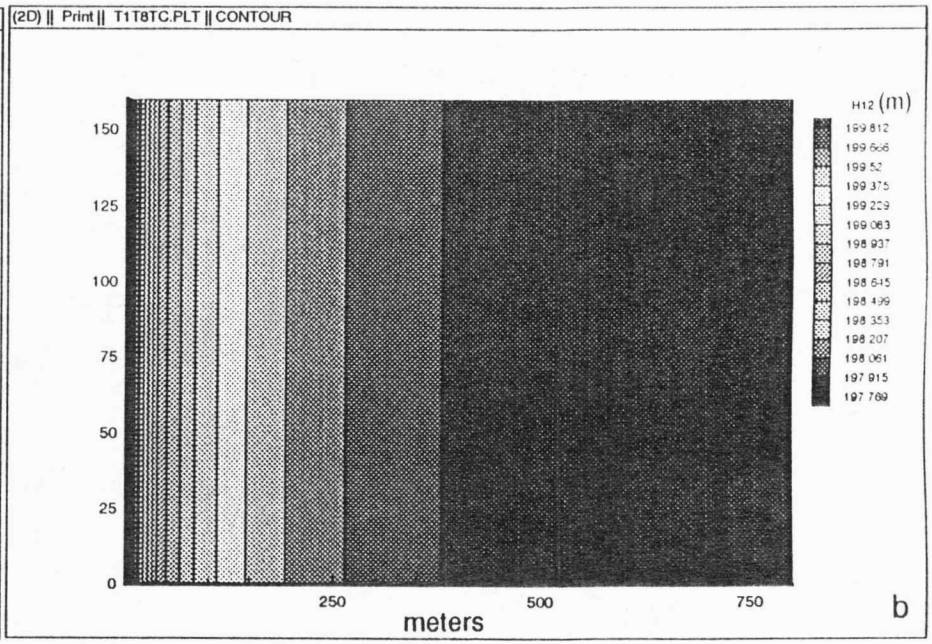
(2D) || Print || T1T8TC.PLT || CONTOUR
H12 (m)
199.812
199.666
199.52
199.375
199.229
199.083
198.937
198.791
198.645
198.499
198.353
198.207
198.061
197.915
197.769
150
125
100
75
50
25
0
250
500
750
meters
b

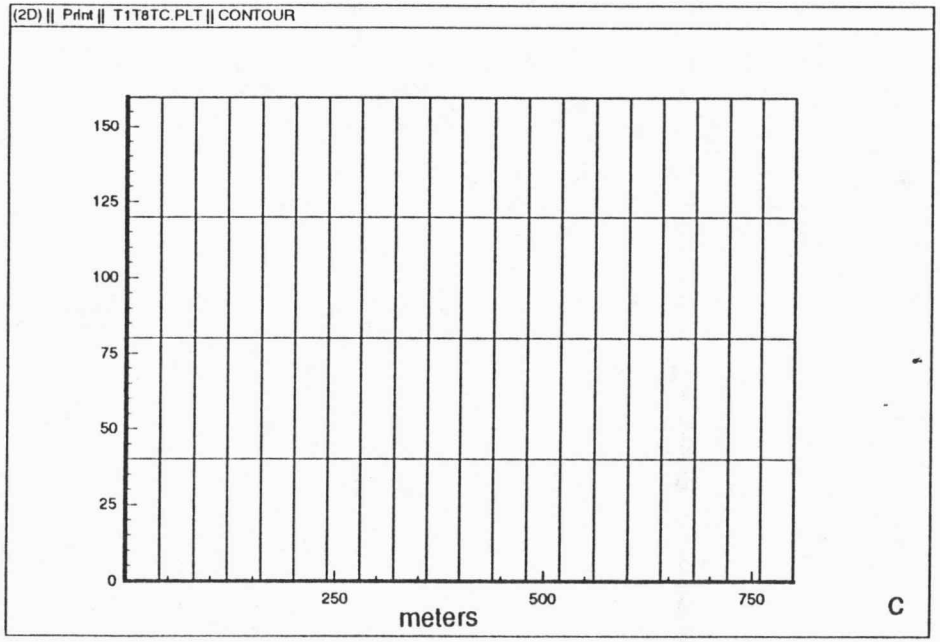
(2D) || Print || T1T8TC.PLT || CONTOUR
150
125
100
75
50
25
0
250
500
750
meters
c

Figure 3

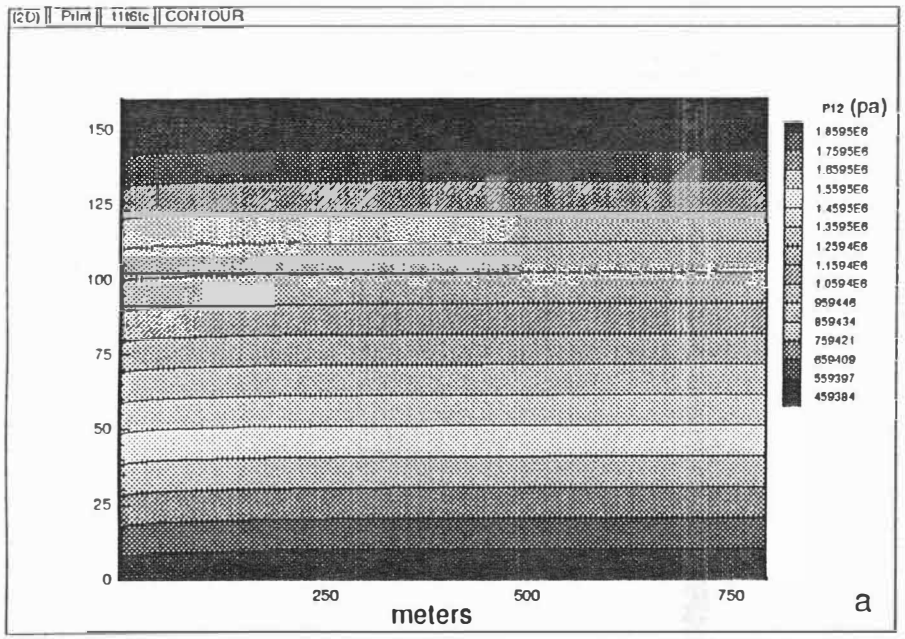
(2D) Print t116tc CONTOUR
P12 (pa)
1.8595E6
1.7595E6
1.6595E6
1.5595E6
1.4595E6
1.3595E6
1.2594E6
1.1594E6
1.0594E6
959446
859434
759421
659409
559397
459384
150
125
100
75
50
25
0
250
500
750
meters
a

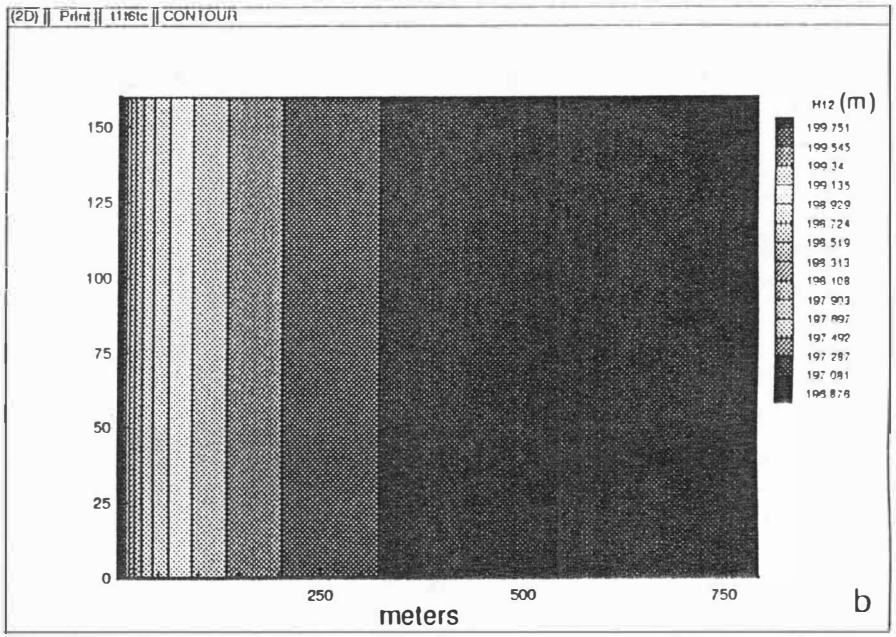
(2D) Print t116tc CONTOUR
H12 (m)
199 751
199 545
199 34
199 135
198 929
198 724
198 519
198 313
198 108
197 903
197 697
197 492
197 287
197 081
196 876
150
125
100
75
50
25
0
250
500
750
meters
b

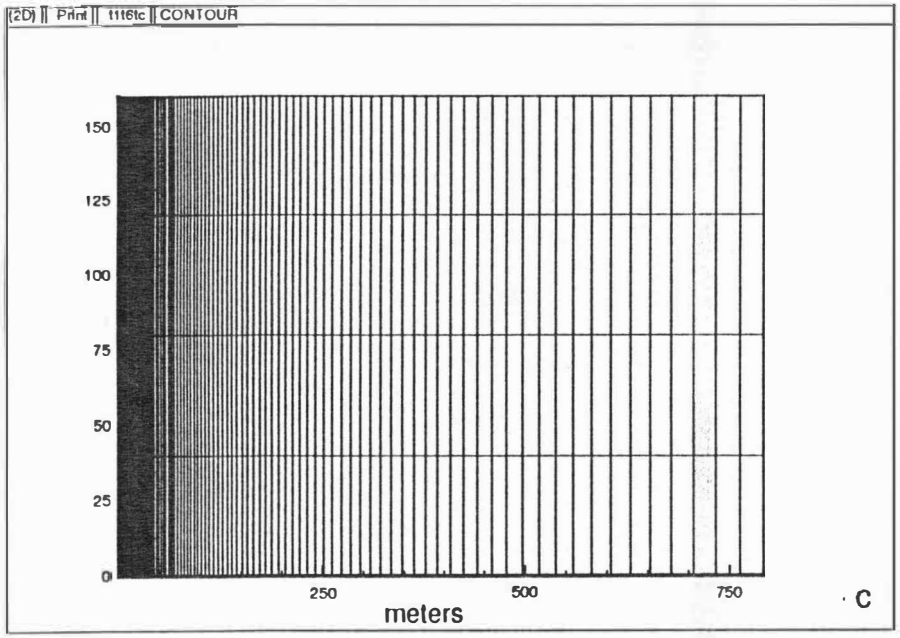
(2D) Print t116tc CONTOUR
150
125
100
75
50
25
0
250
500
750
meters
c

Figure 4

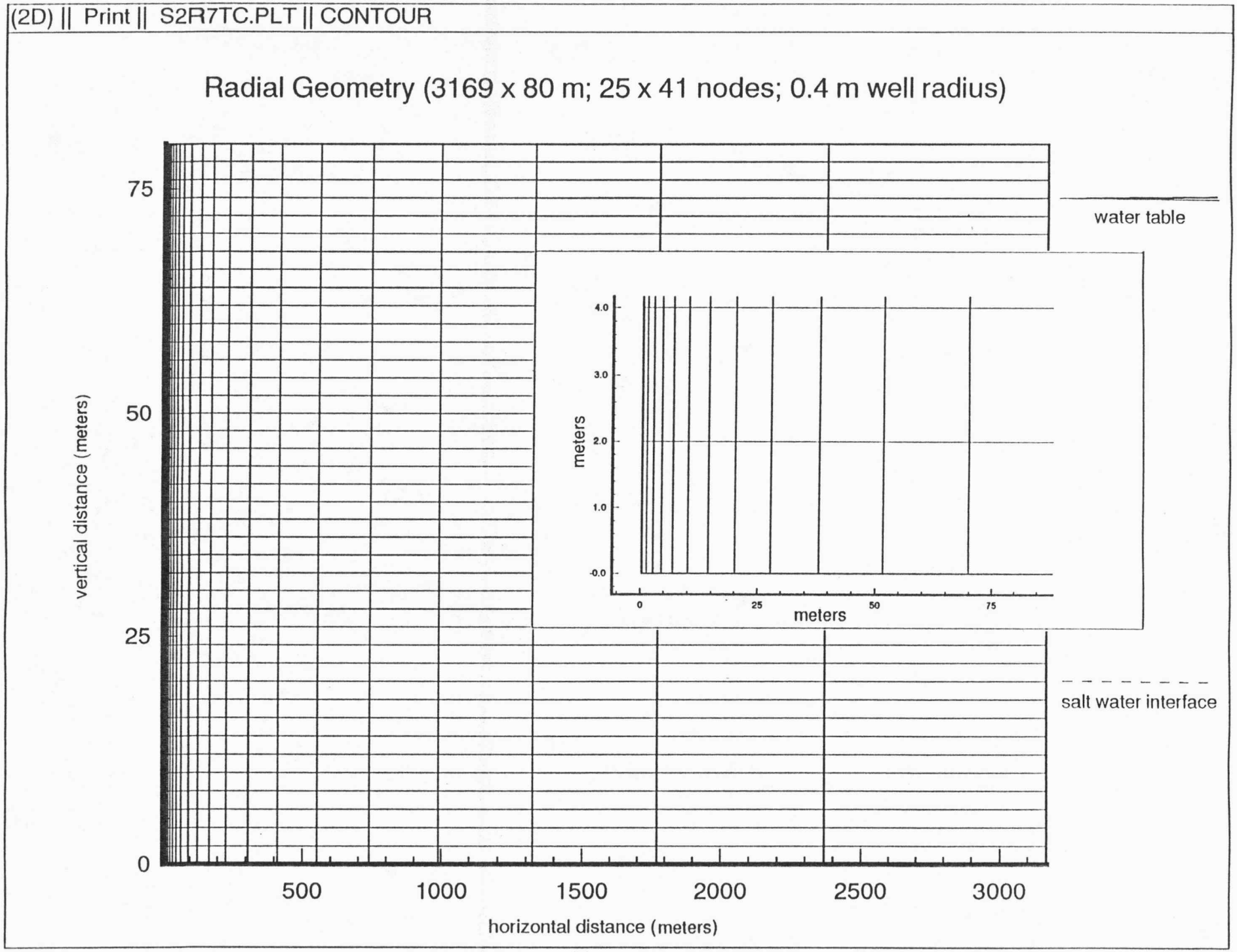
(2D) || Print || S2R7TC.PLT || CONTOUR
Radial Geometry (3169 x 80 m; 25 x 41 nodes; 0.4 m well radius)
vertical distance (meters)
75
50
25
0
500
1000
1500
2000
2500
3000
horizontal distance (meters)
water table
salt water interface
meters
4.0
3.0
2.0
1.0
-0.0
0
25
50
75
meters

Figure 5

(2D) || Print || S2R7TC.PLT || CONTOUR

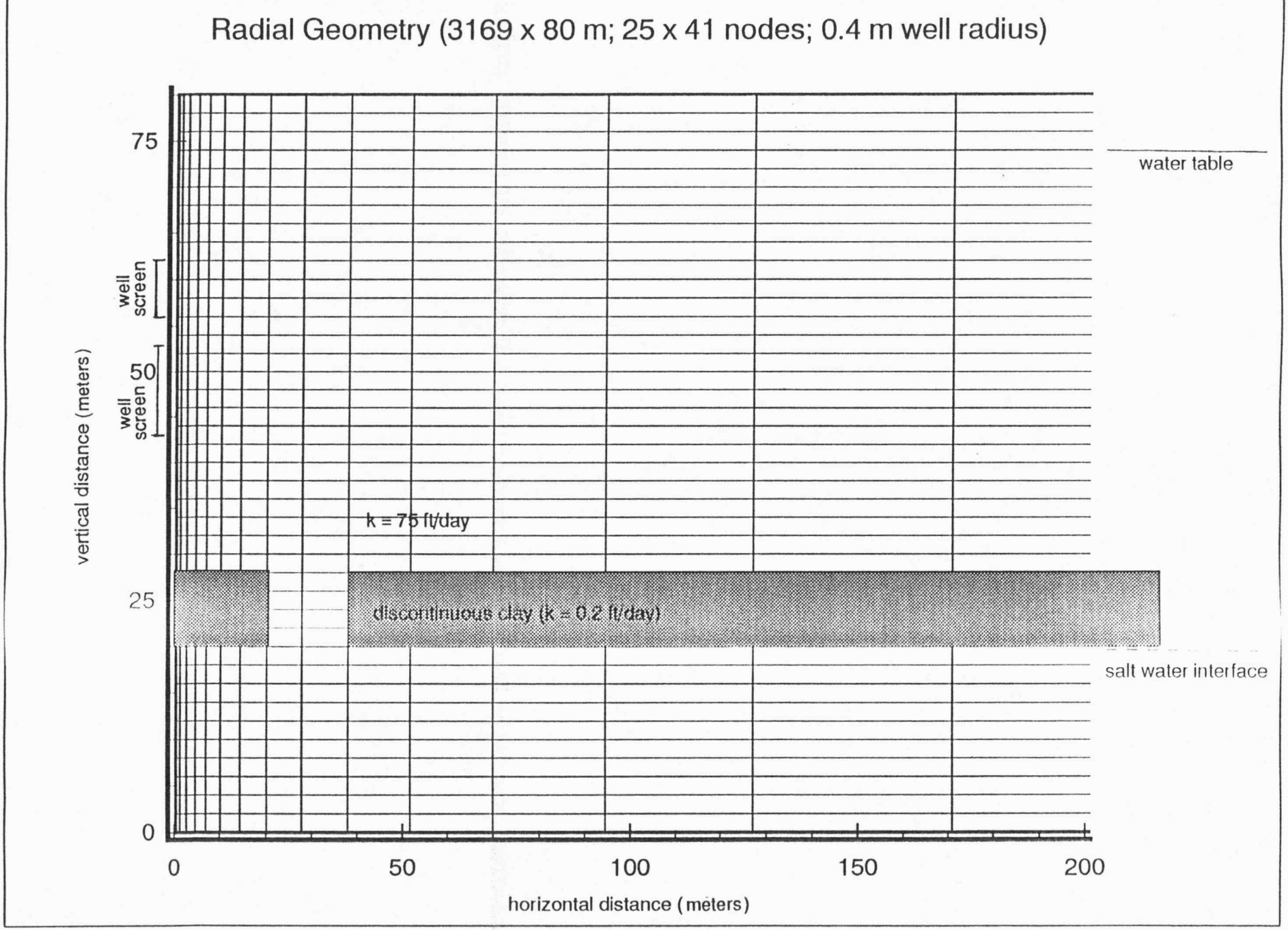

Figure 6

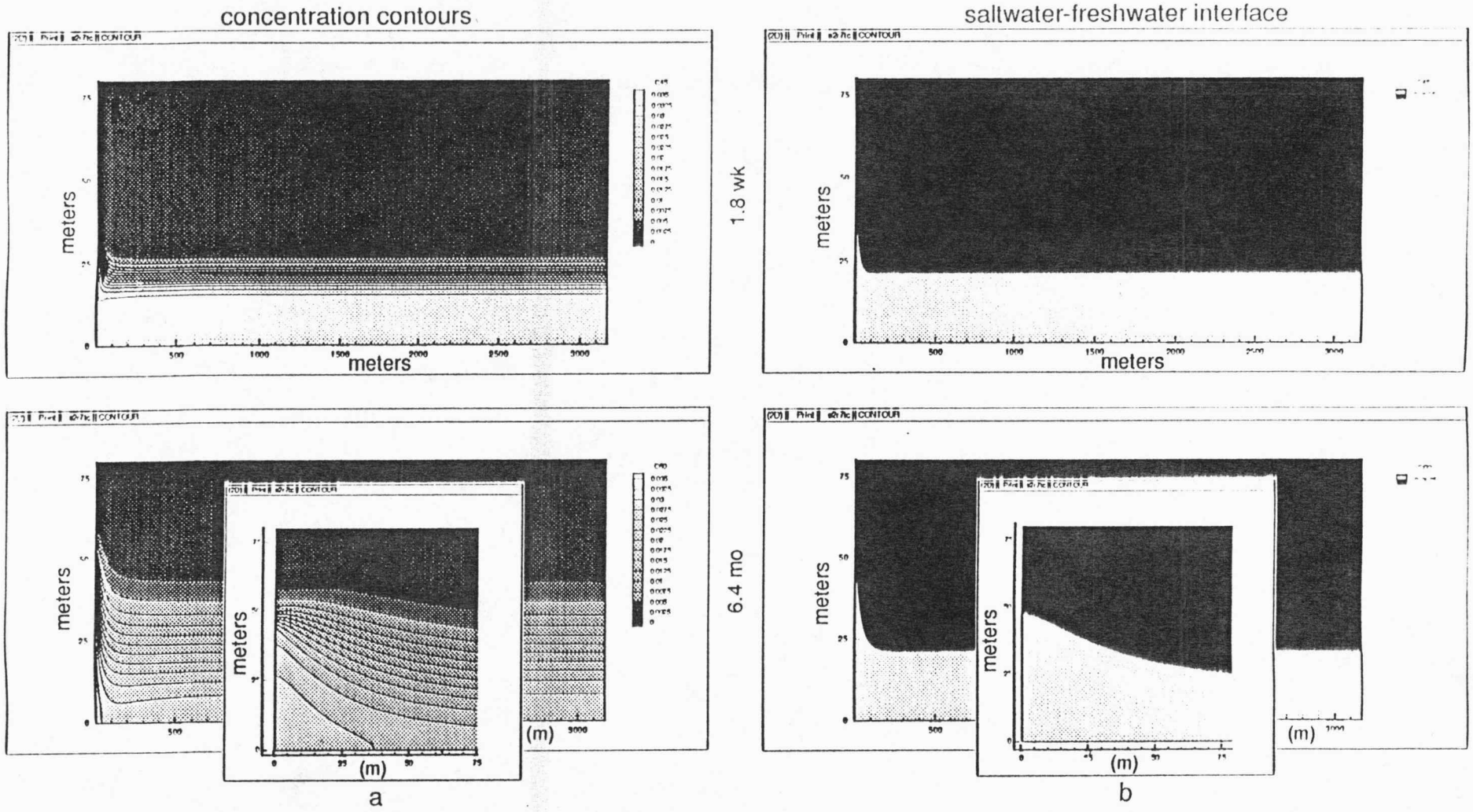

Figure 7. Case 1

Base case: single, homogeneous alluvial aquifer (K_{aq}=75 ft/d; S_{aq}=0.15; α_L=10m; no flow bottom boundary conditions). Well pumping continuously at 800 gpm.

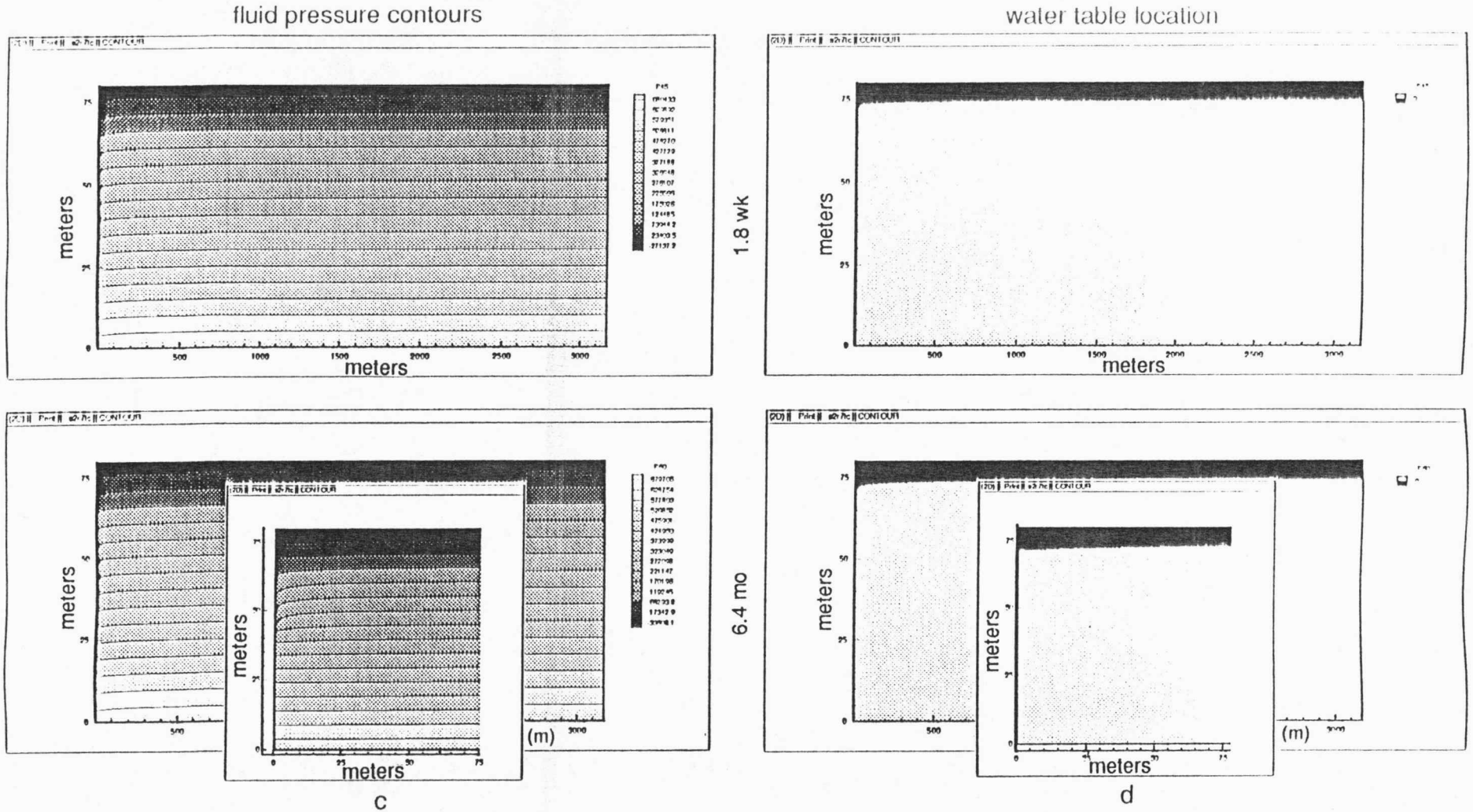

Figure 7 (continued)

Base case: single, homogeneous alluvial aquifer (K_{aq}=75 ft/d; S_{aq}=0.15; α_L=10m; no flow bottom boundary conditions). Well pumping continuously at 800 gpm

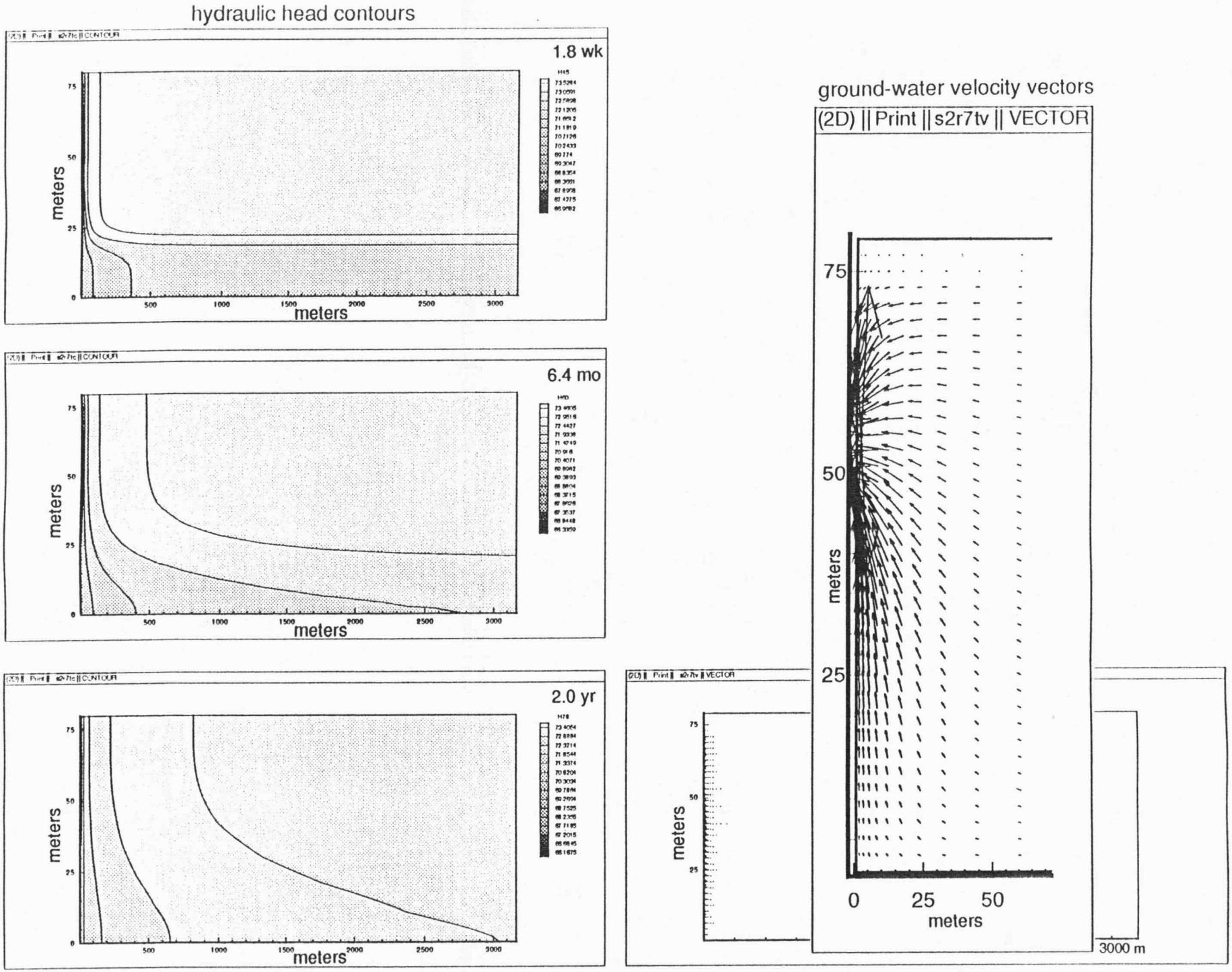

Figure 7 (continued)

Base case: single, homogeneous alluvial aquifer (K_{aq}=75 ft/d; S_{aq}=0.15; α_L=10m; no flow bottom boundary conditions). Well pumping continuously at 800 gpm.

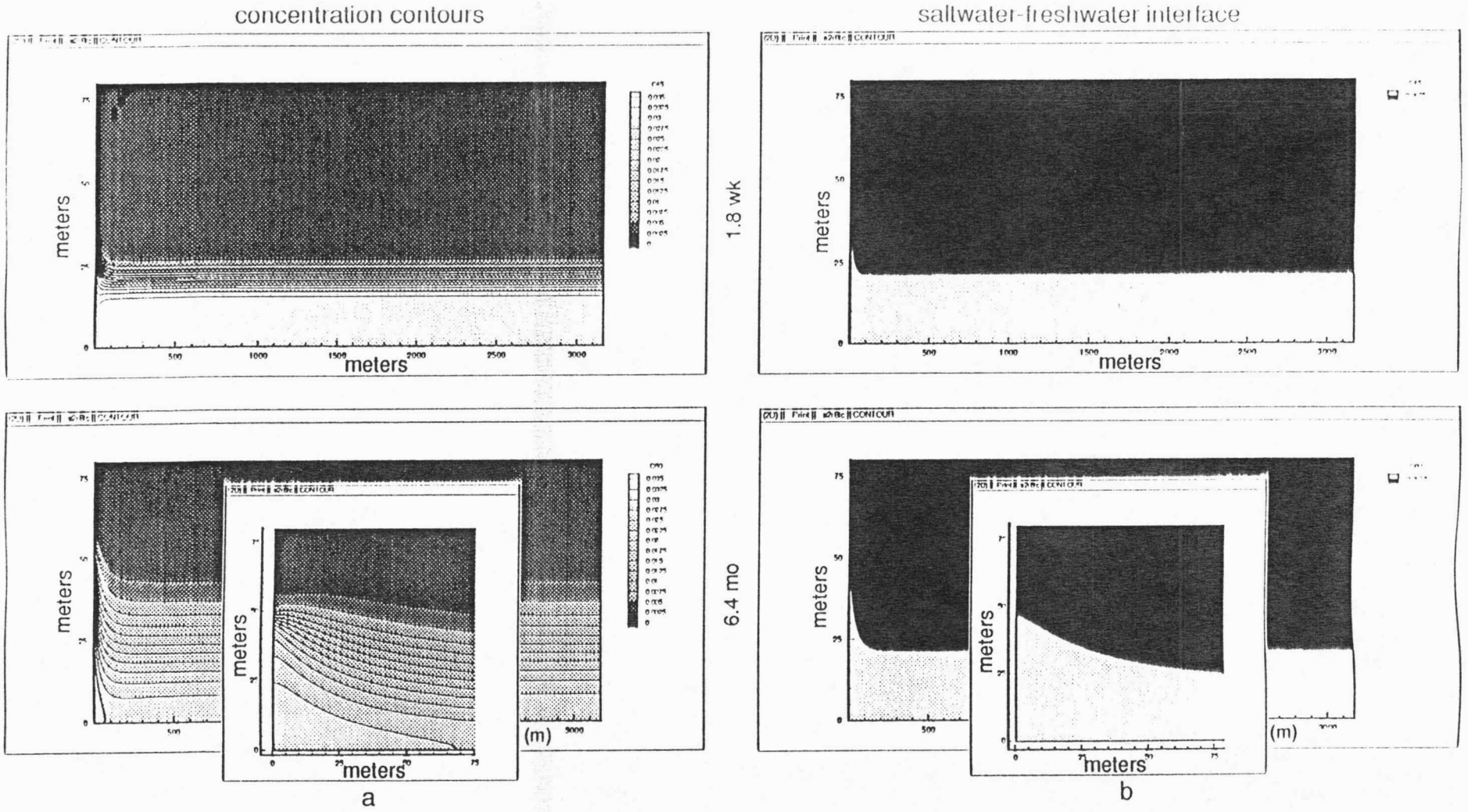

Figure 8. Case 2

Base case with continuous pumping reduced to 200 gpm.

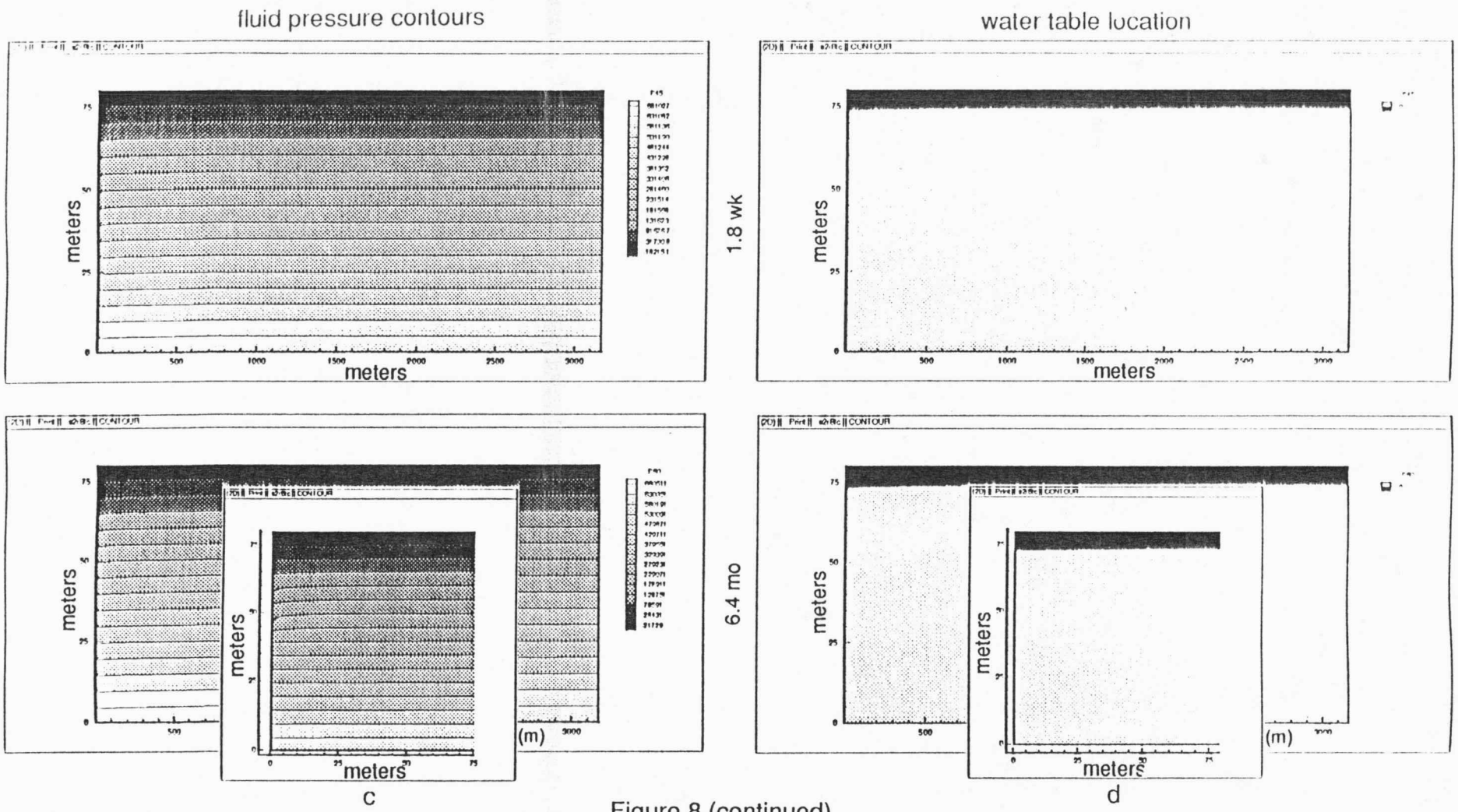

Figure 8 (continued)

Base case with continuous pumping reduced to 200 gpm.

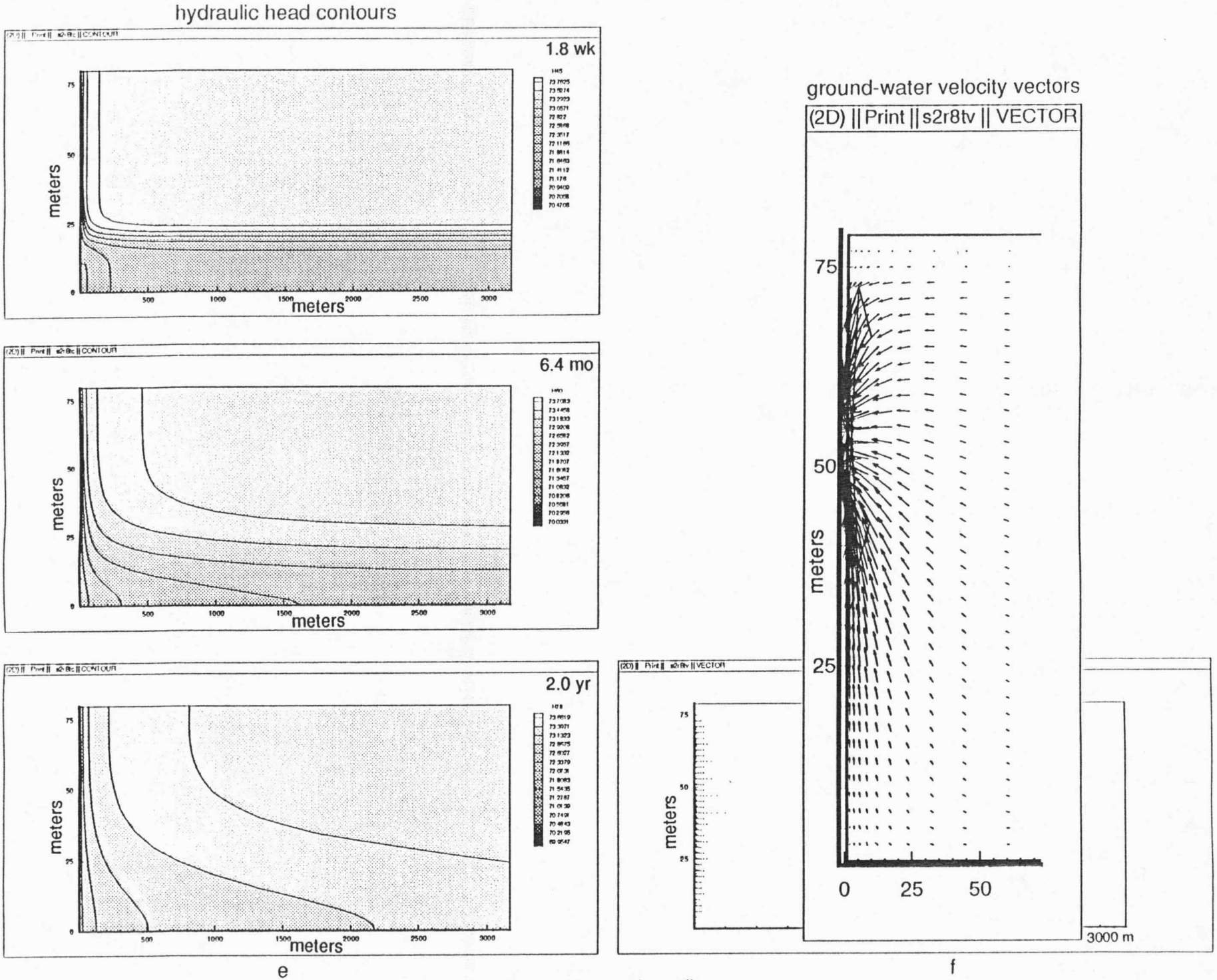

Figure 8 (continued)

Base case with continuous pumping reduced to 200 gpm.

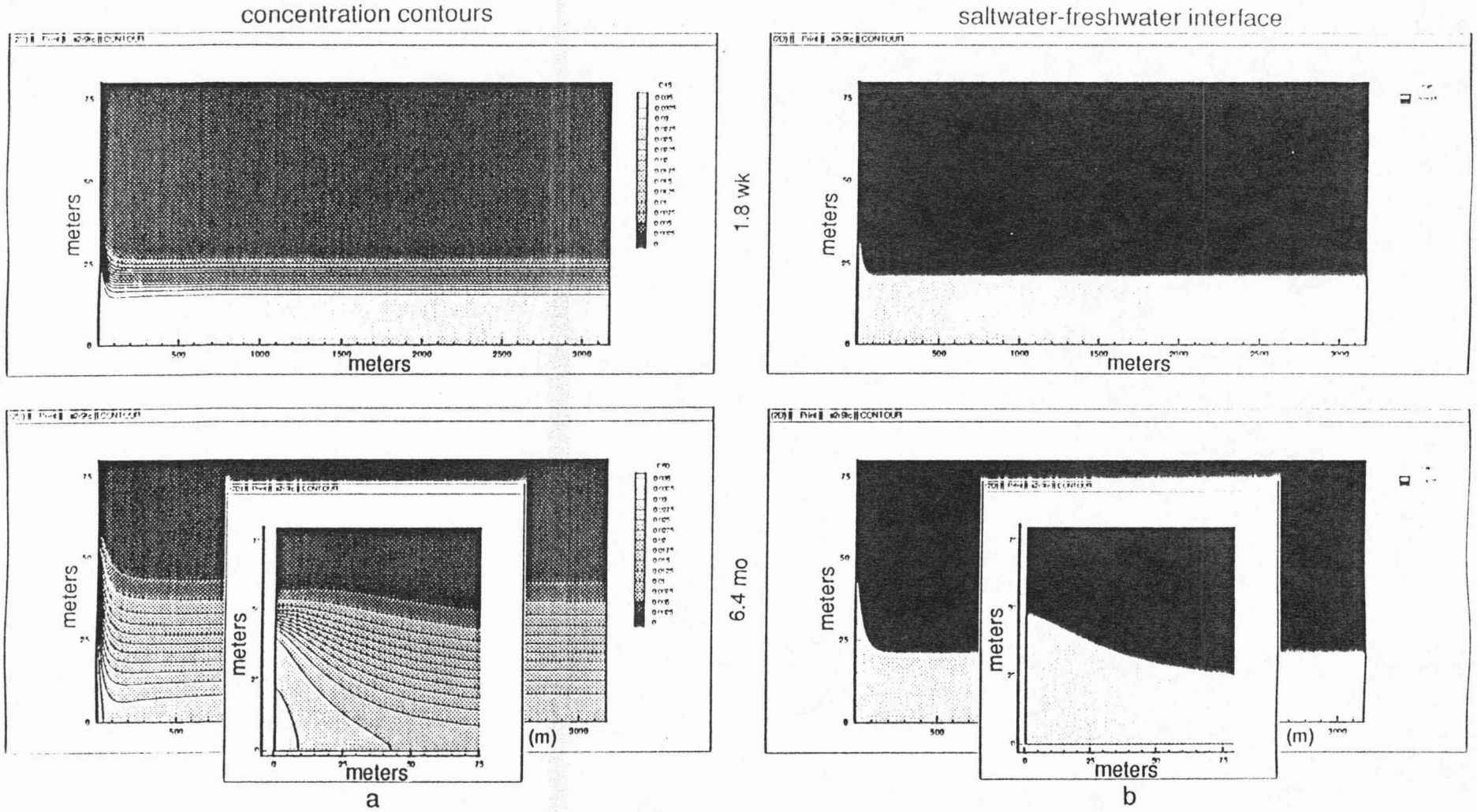

Figure 9. Case 3

Base case with longitudinal dispersivity α_L reduced to 1m.

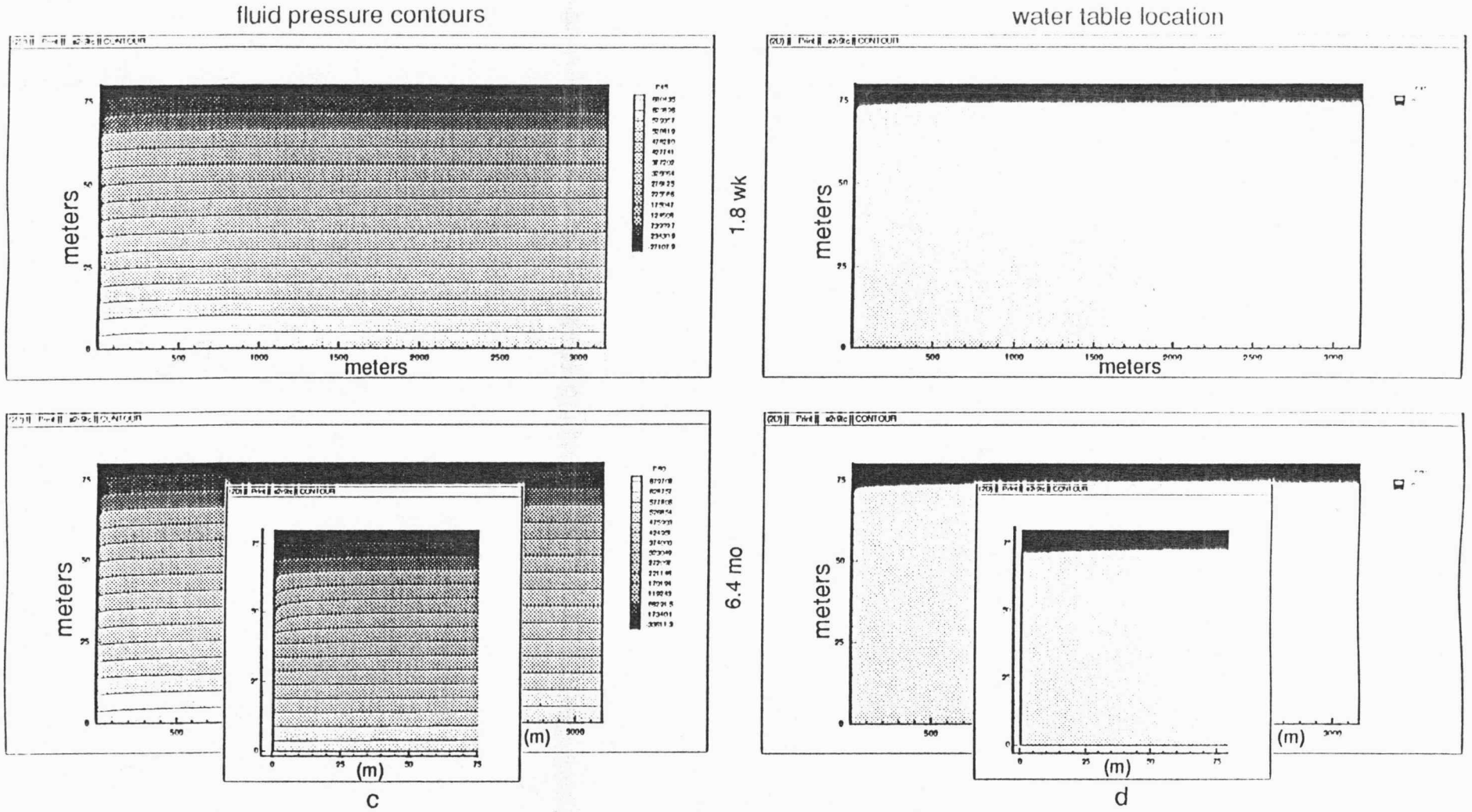

Figure 9 (continued)

Base case with longitudinal dispersivity α_L reduced to 1m.

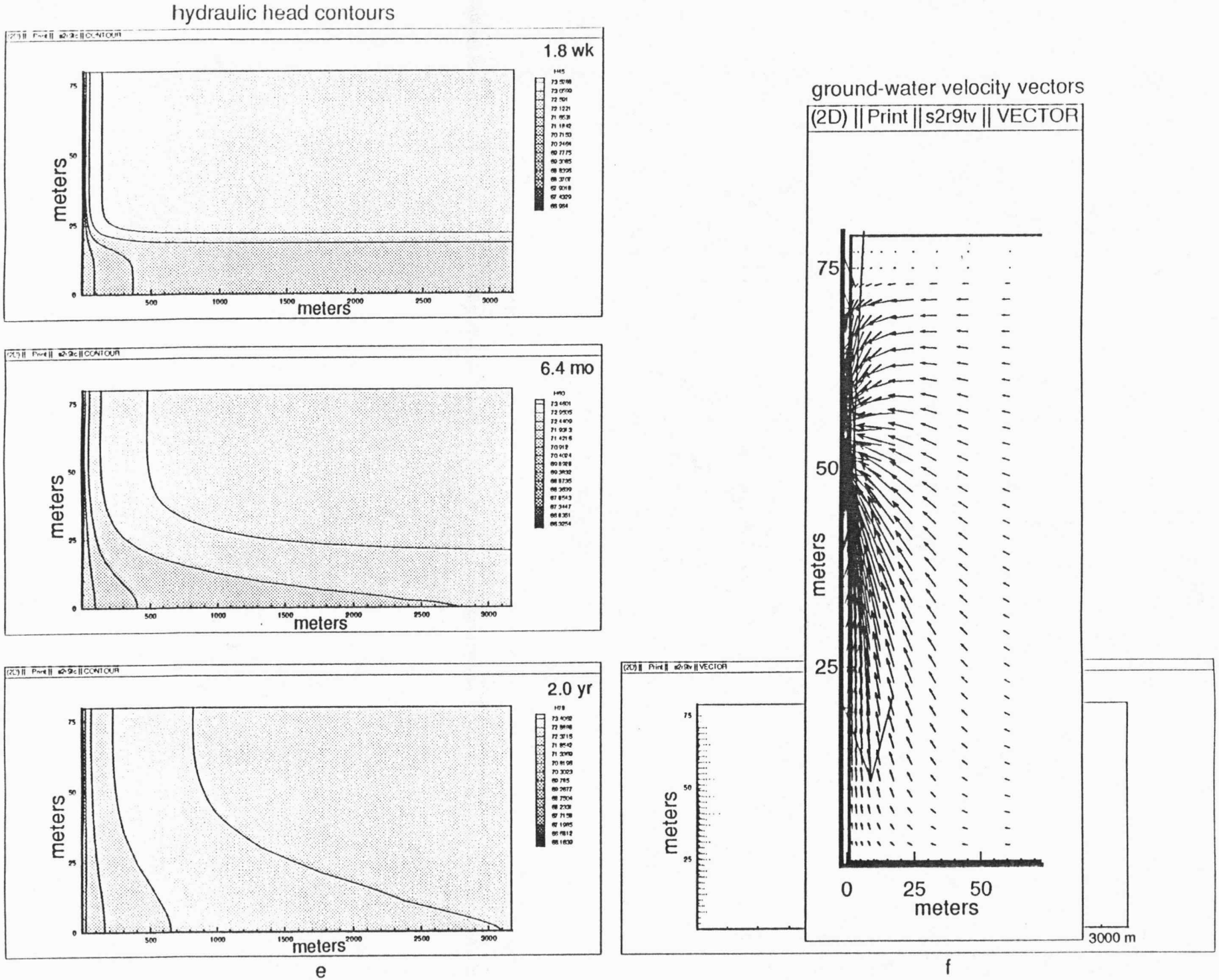

Figure 9 (continued)

Base case with longitudinal dispersivity α_L reduced to 1m.

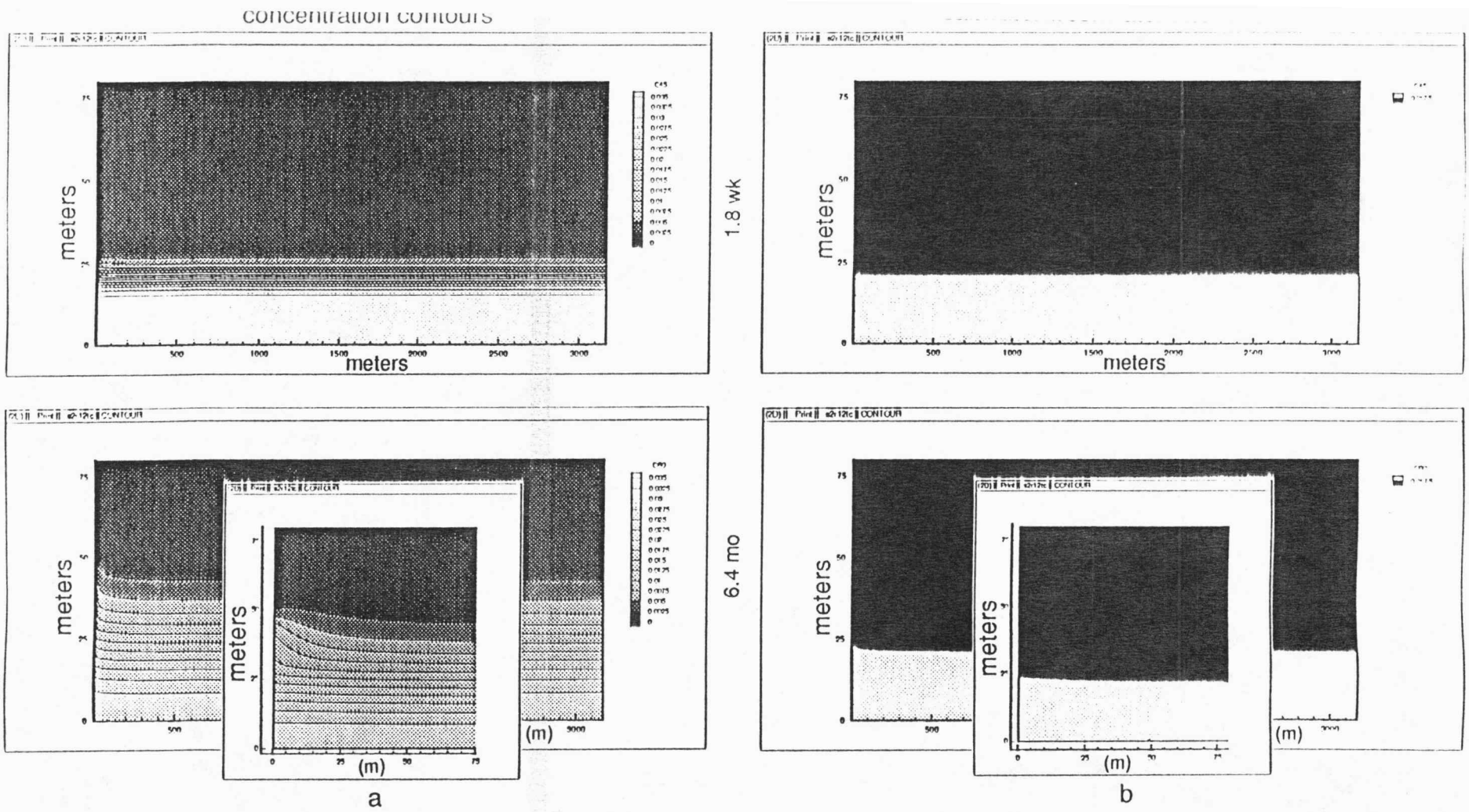

Figure 10. Case 4

Singular aquifer with a continuous clay layer (K_{CL}=0.2 ft/d; S_{CL}=0.15) overlying the initial saltwater-freshwater interface

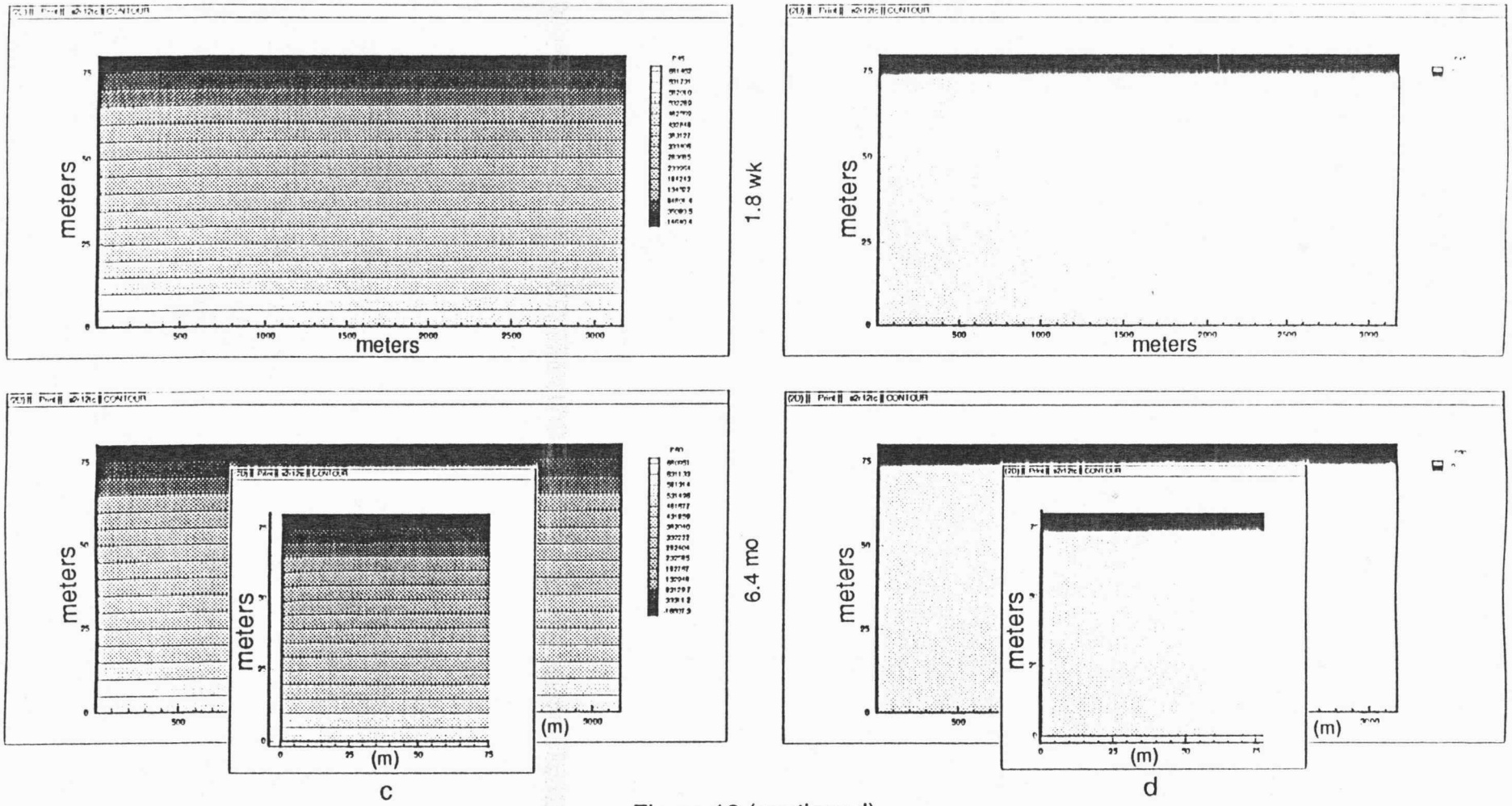

Figure 10 (continued)

Singular aquifer with a continuous clay layer (K_{CL}=0.2 ft/d; S_{CL}=0.15) overlying the initial saltwater-freshwater interface

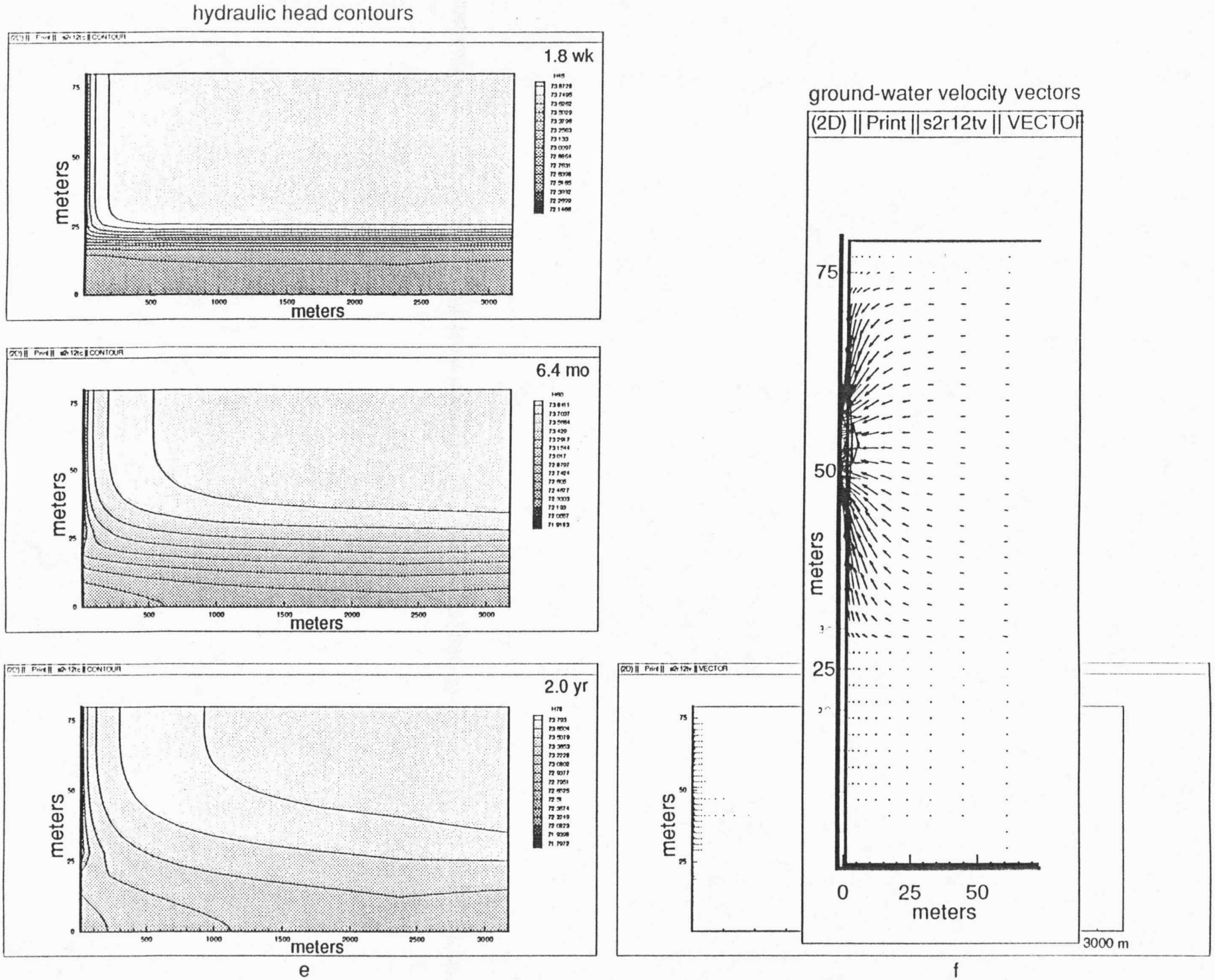

Figure 10 (continued)

Singular aquifer with a continuous clay layer (K_{CL}=0.2 ft/d; S =0.15) overlying the initial saltwater-freshwater interface

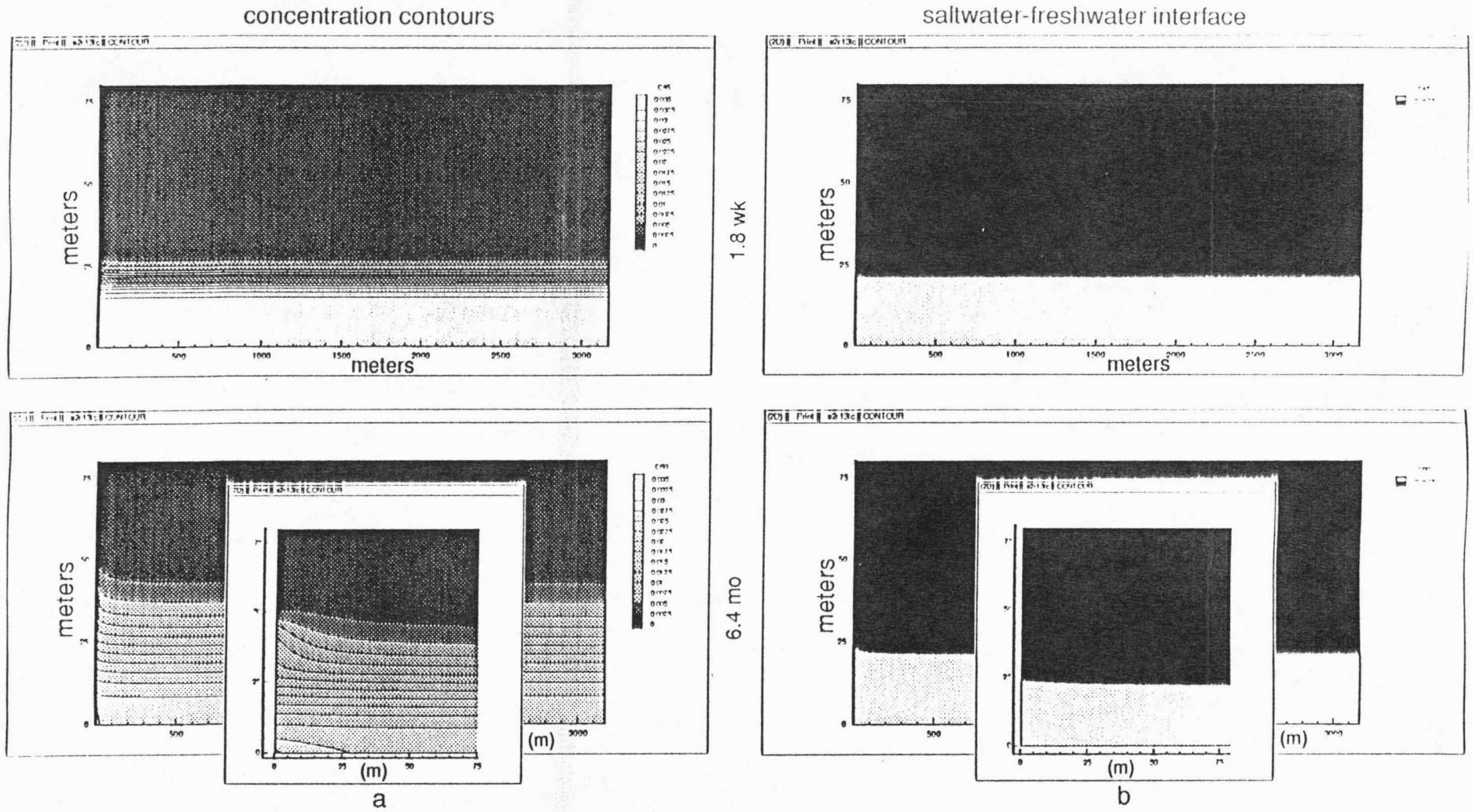

Figure 11. Case 5

Single aquifer with a continuous clay layer but with clay storativity, S_{CL} reduced to 0.075.

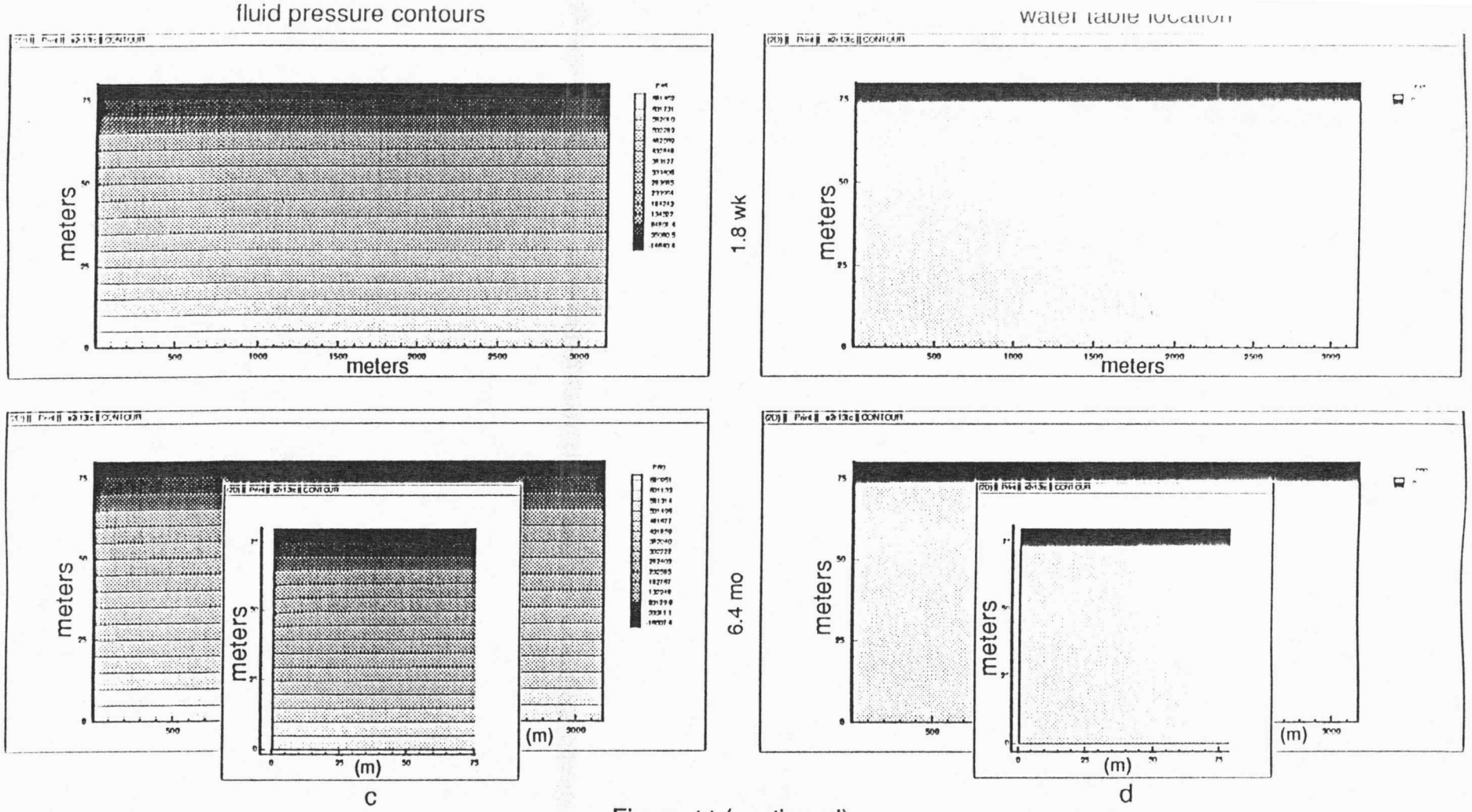

Figure 11 (continued)

Single aquifer with a continuous clay layer but with clay storativity, S_{CL} reduced to 0.075.

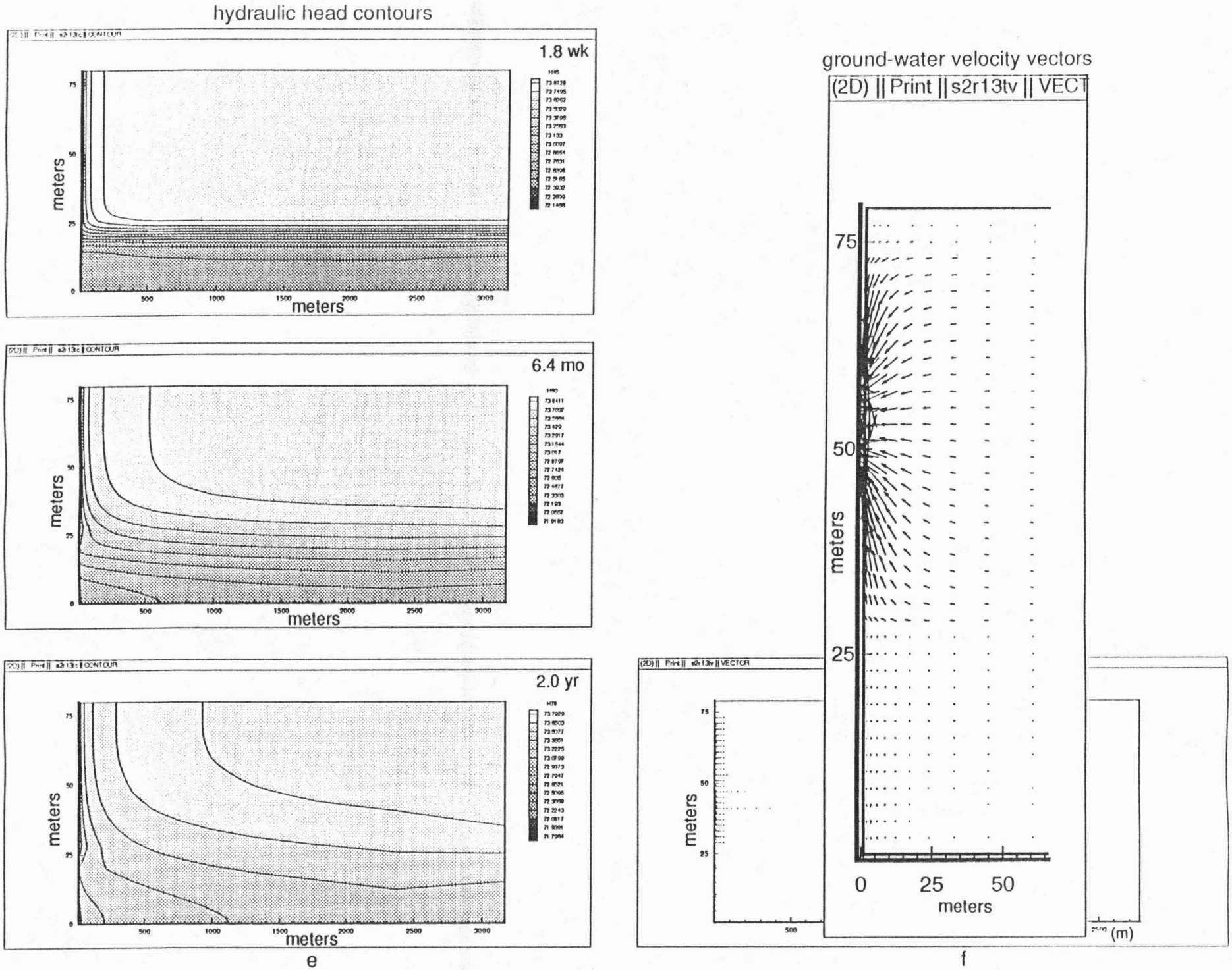

Figure 11 (continued)

Single aquifer with a continuous clay layer but with clay storativity, S_{CL} reduced to 0.075.

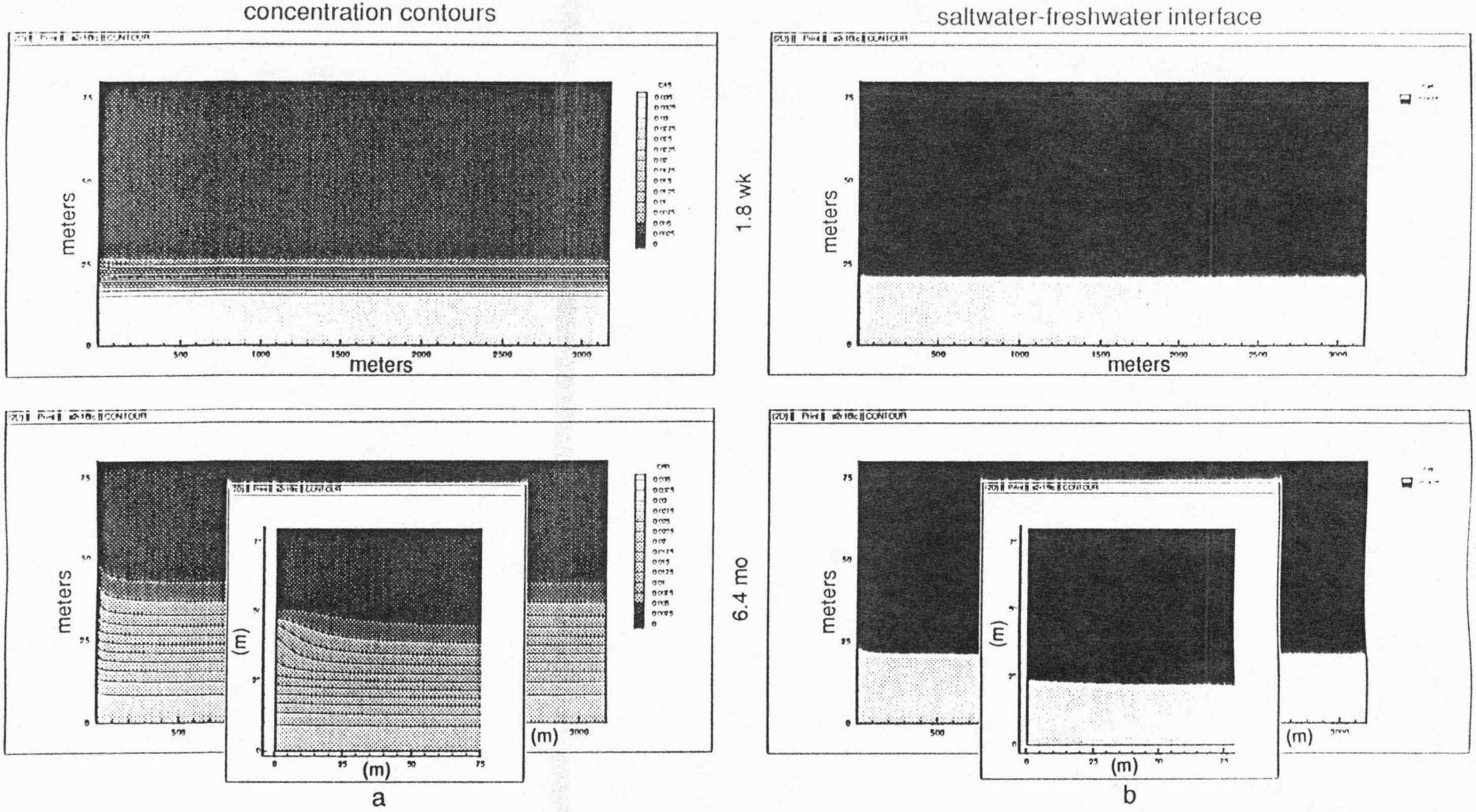

Figure 12. Case 6

Single aquifer with a continuous clay layer but with $S_{aq} = S_{CL} = 0.075$

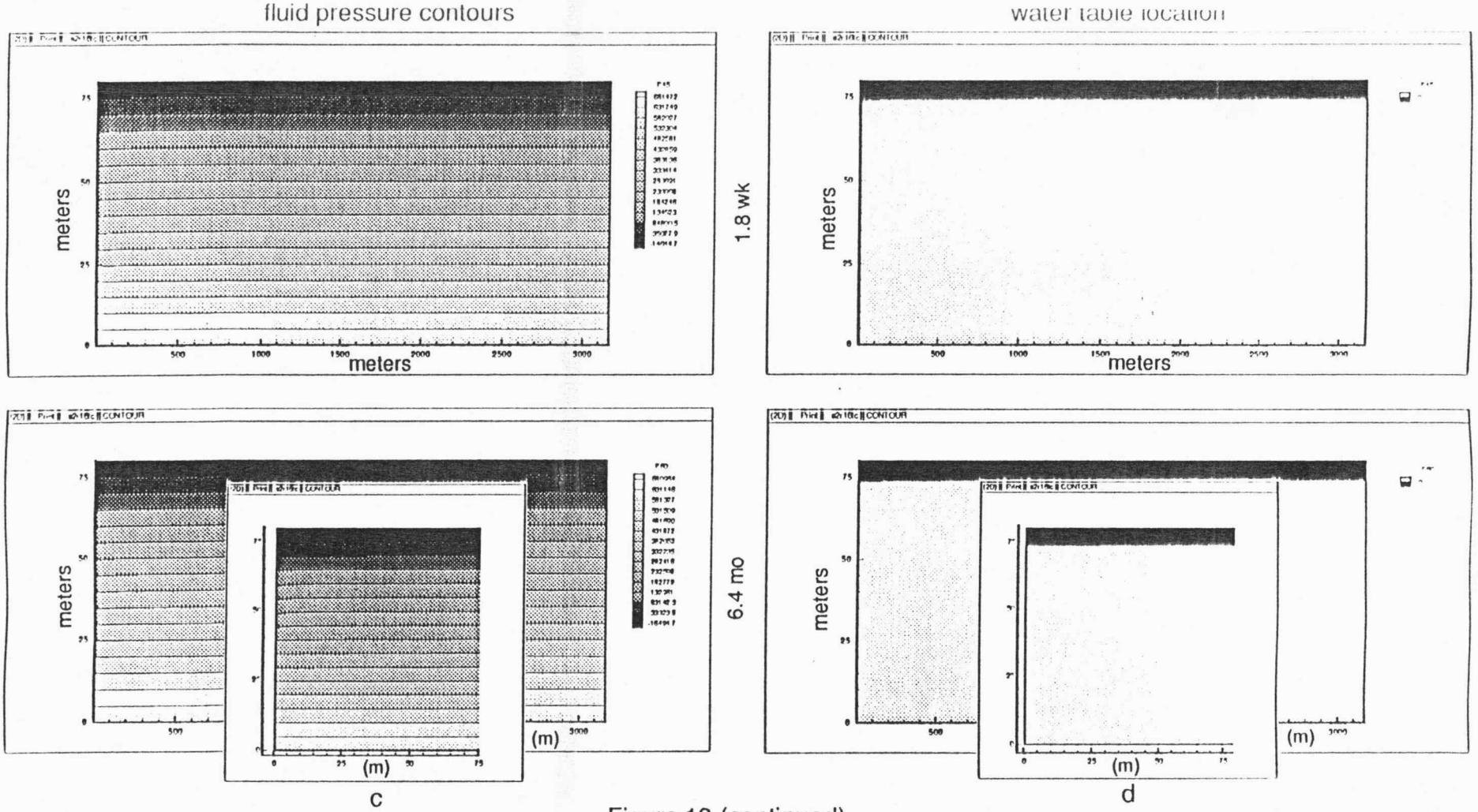

Figure 12 (continued)

Single aquifer with a continuous clay layer but with $S_{aq} = S_{CL} = 0.075$

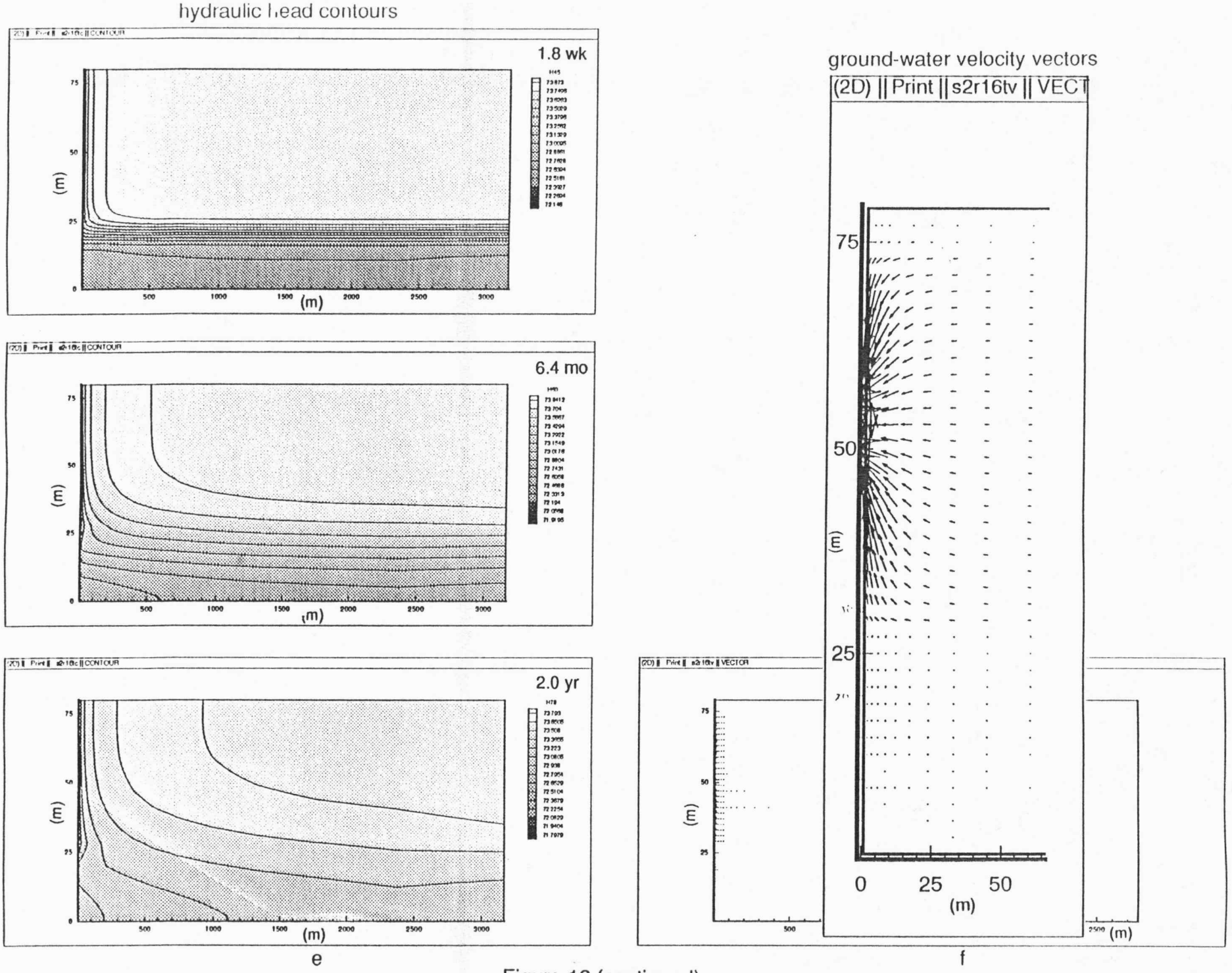

Figure 12 (continued)

Single aquifer with a continuous clay layer but with $S_{aq} = S_{CL} = 0.075$

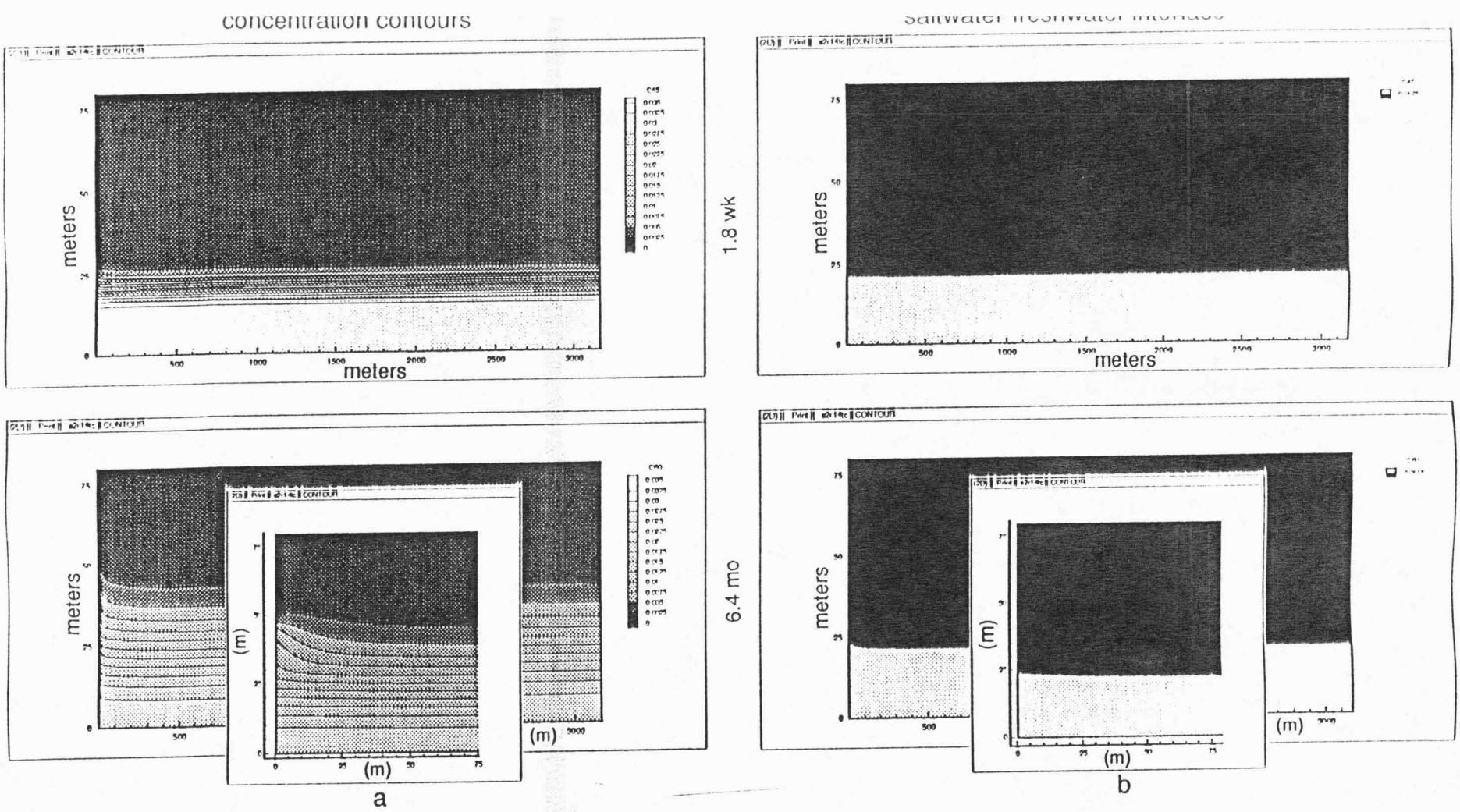

Figure 13. Case 7

Single aquifer with a continuous clay layer but with specified bottom boundary brine concentration

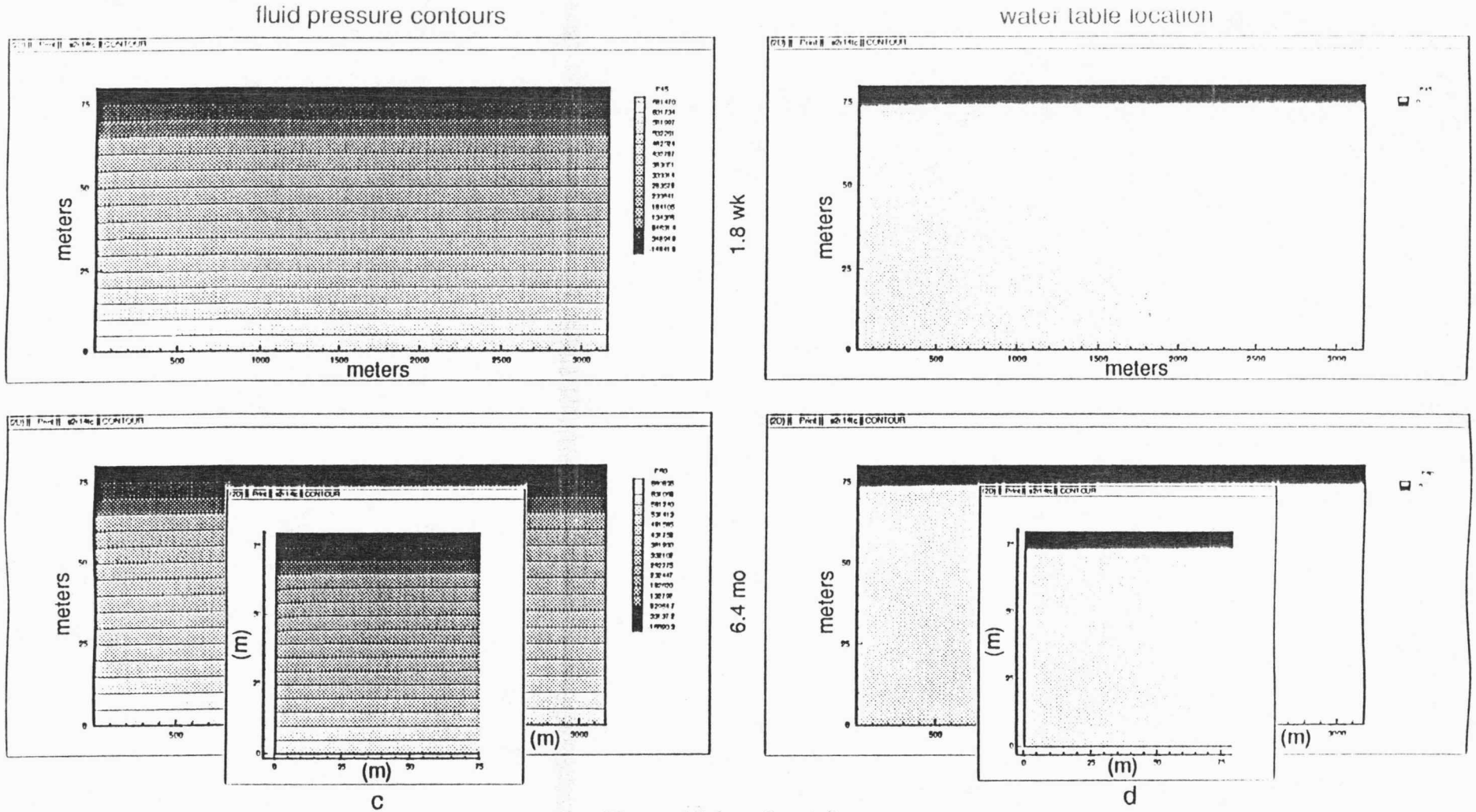

Figure 13 (continued)

Single aquifer with a continuous clay layer but with specified bottom boundary brine concentration

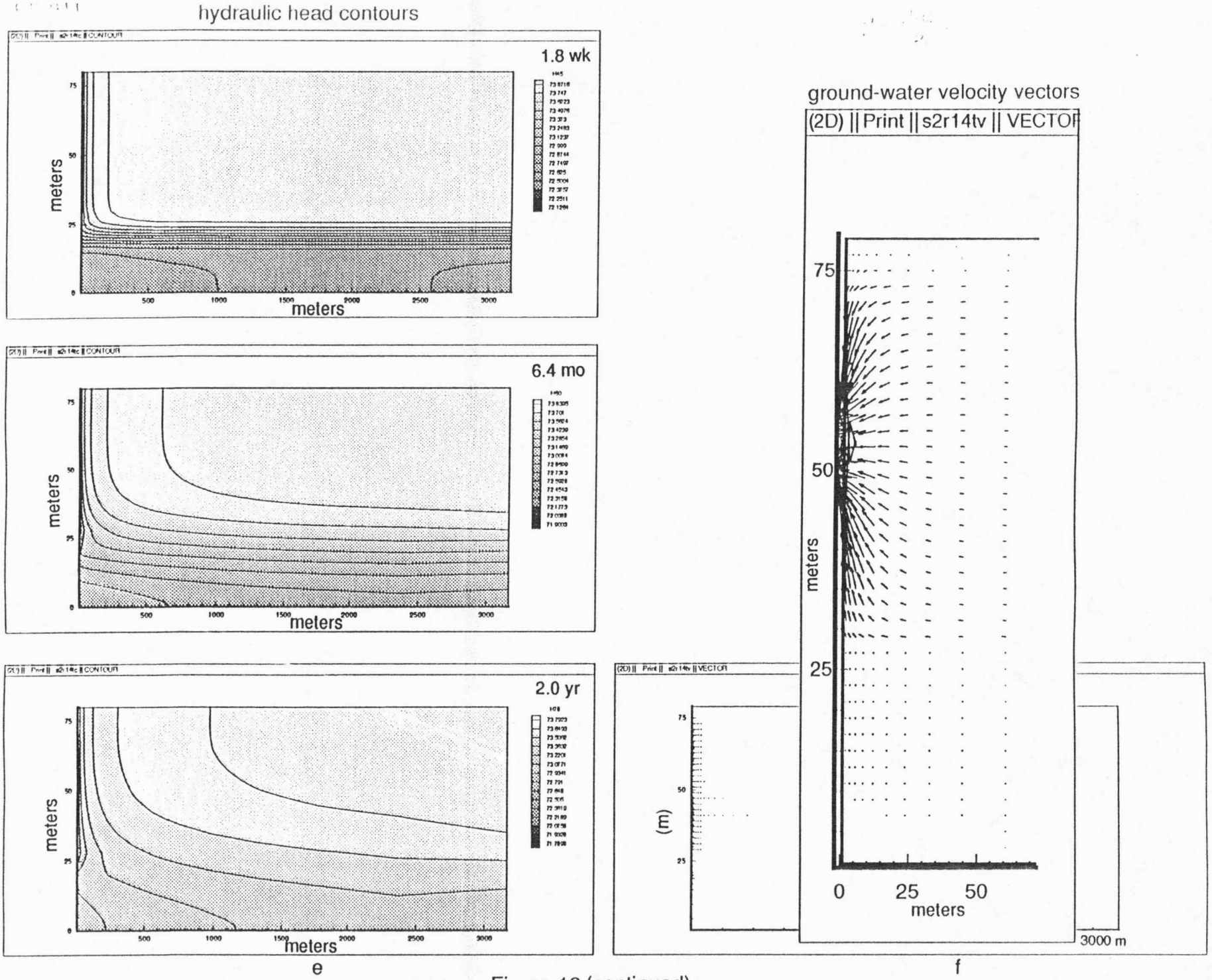

Figure 13 (continued)

Single aquifer with a continuous clay layer but with specified bottom boundary brine concentration

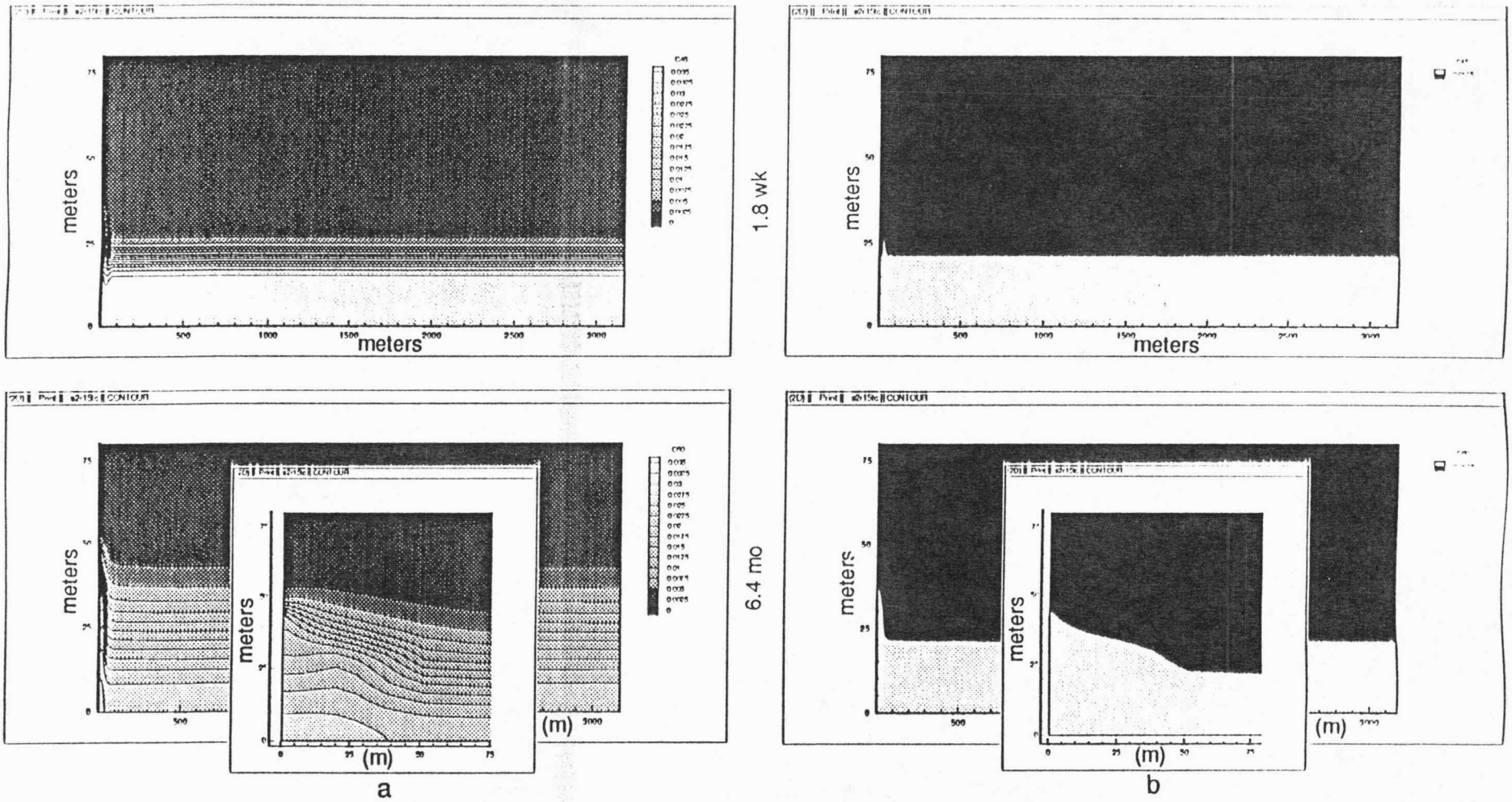

Figure 14. Case 8

Single aquifer with a discontinuous clay layer (K_{CL}=0.2 ft/d; S_{CE} 0.15)

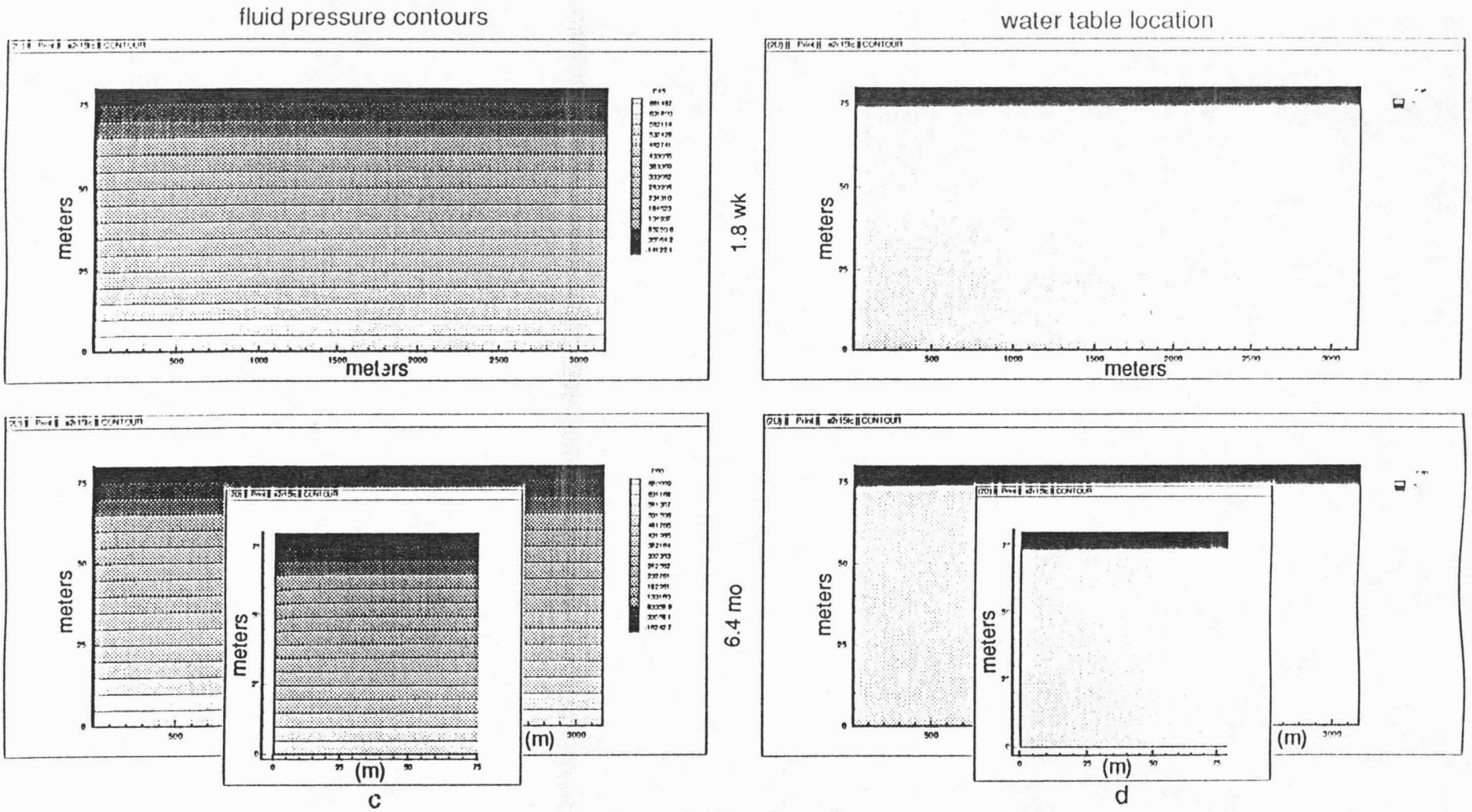

Figure 14 (continued)

Single aquifer with a discontinuous clay layer (K_{CL}=0.2 ft/d; S_{CL}= 0.15)

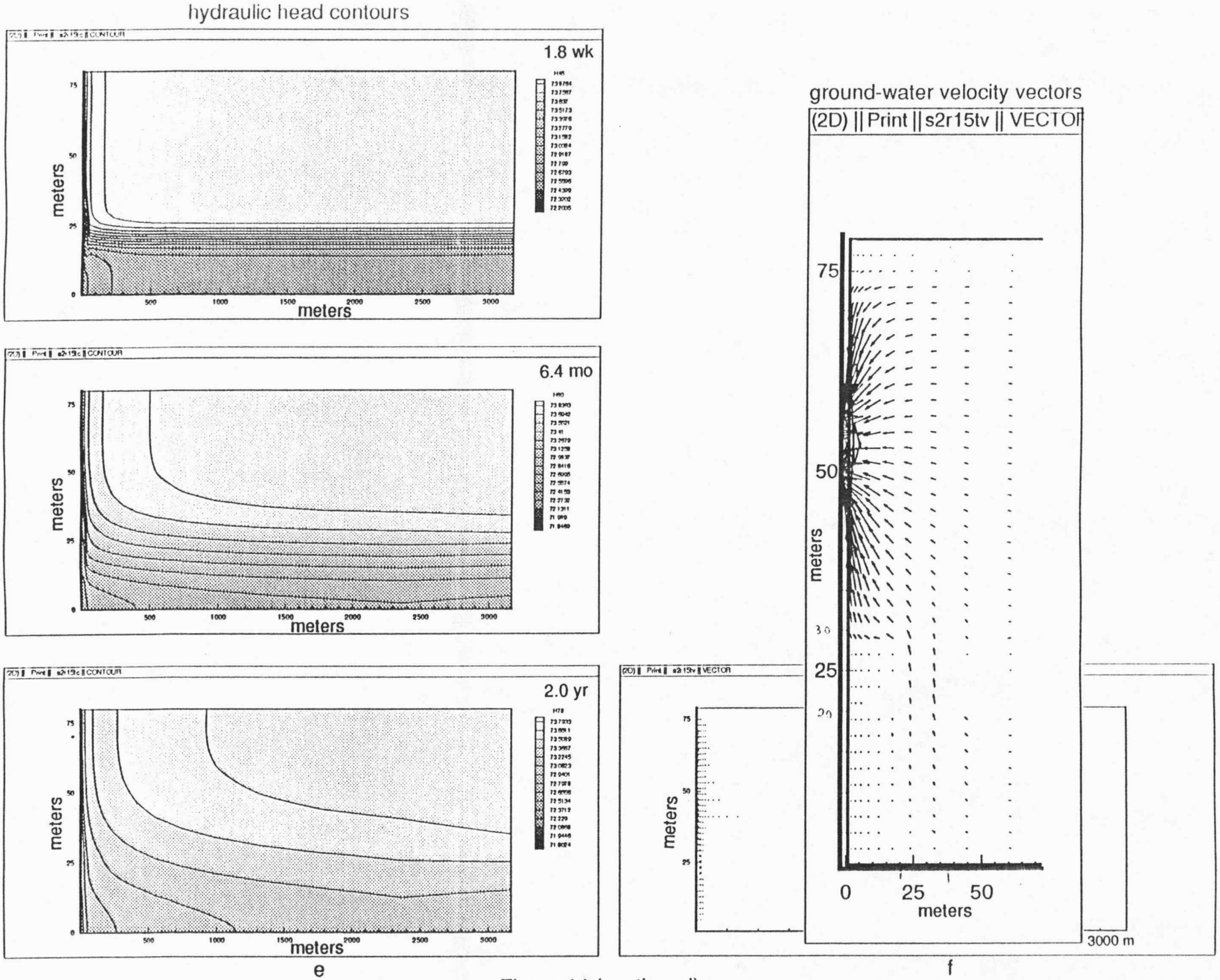

Figure 14 (continued)

Single aquifer with a discontinuous clay layer (K_{CL}=0.2 ft/d; S_{CL}= 0.15)

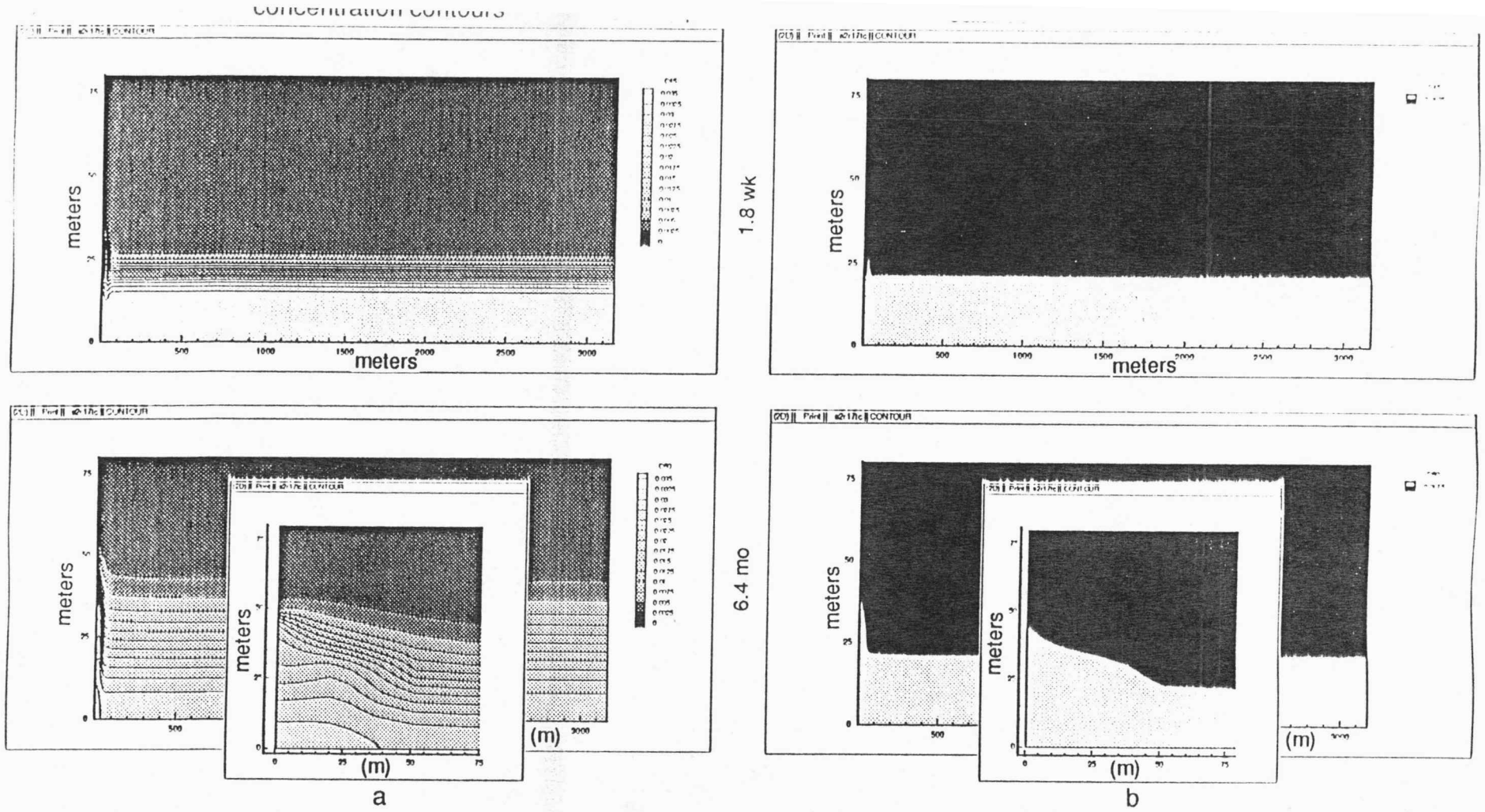

Figure 15. Case 9

Single aquifer with a discontinuous clay layer but with clay storativity reduced to S_{CL}=0.075

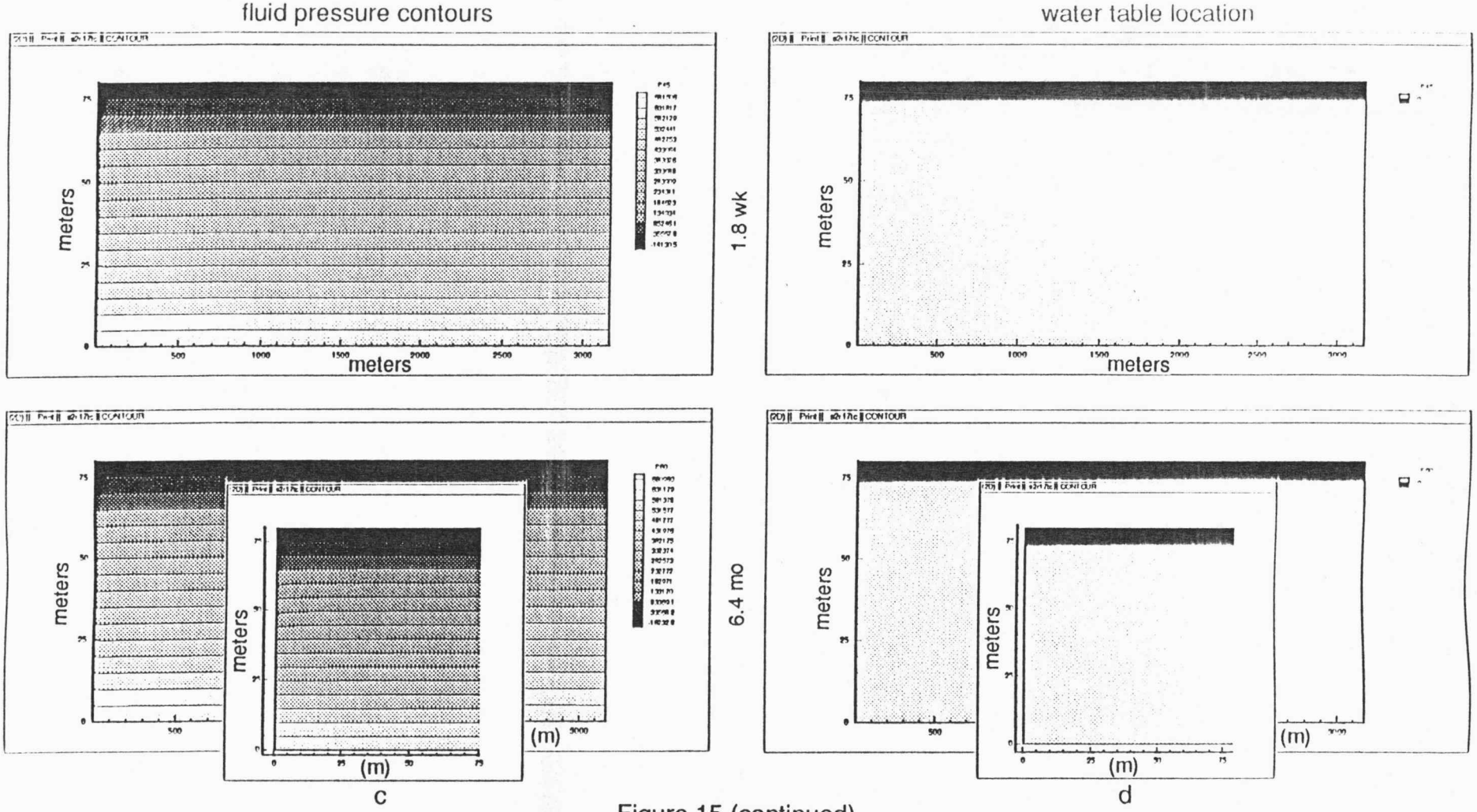

Figure 15 (continued)

Single aquifer with a discontinuous clay layer but with clay storativity reduced to $S_{CL}=0.075$

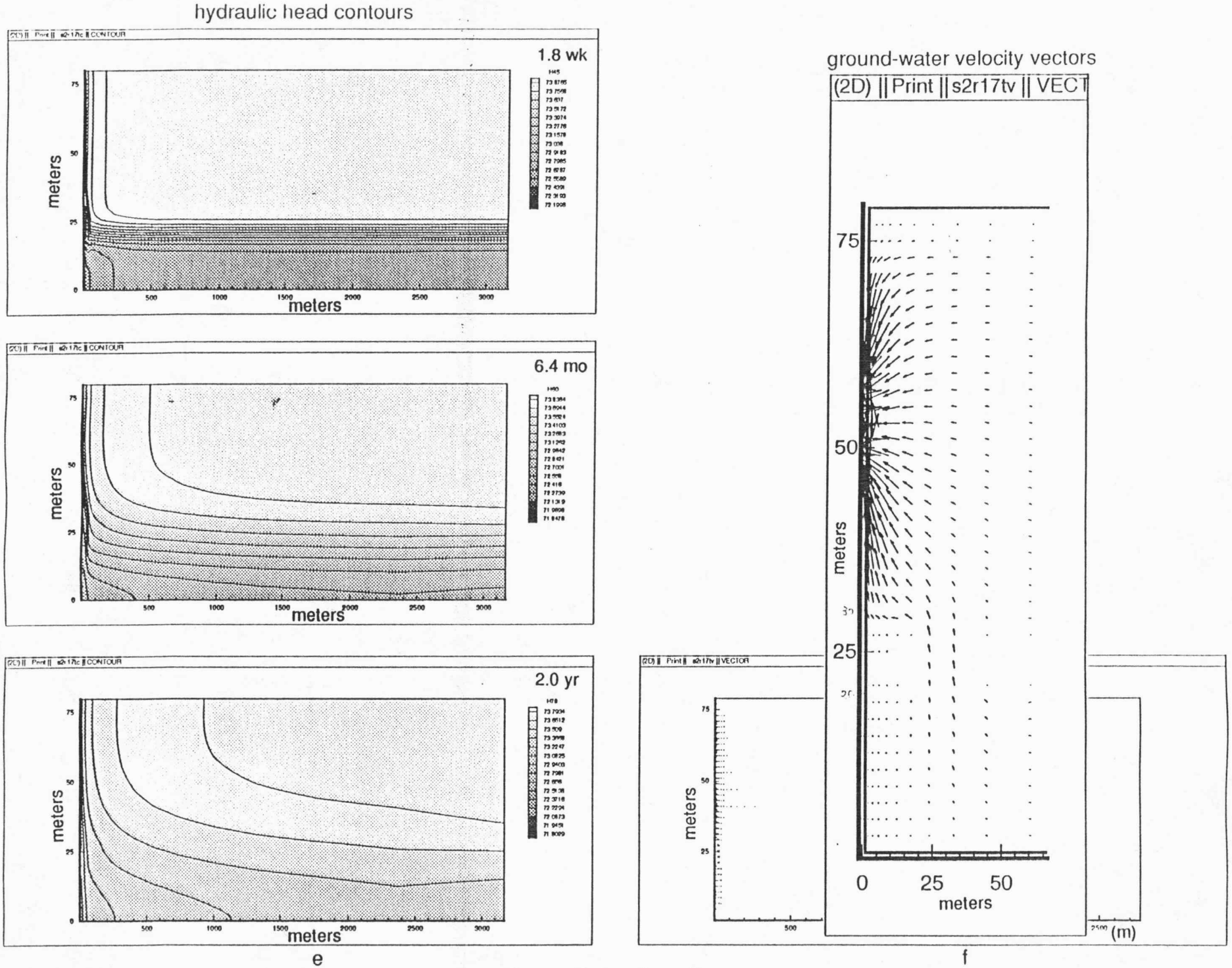

Figure 15 (continued)

Single aquifer with a discontinuous clay layer but with clay storativity reduced to S_{CL}=0.075

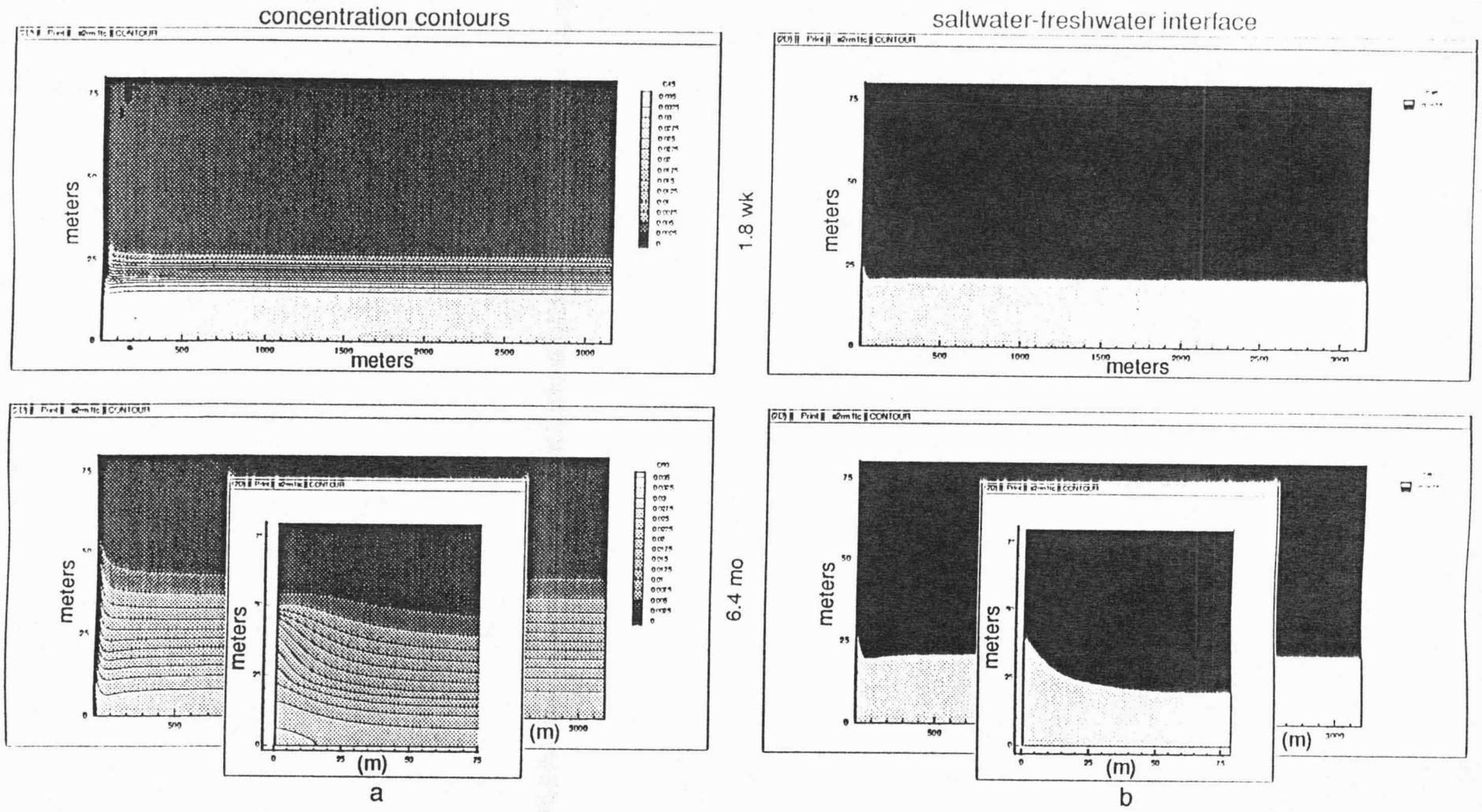

Figure 16. Case 10

Layered aquifer system: Base case alluvial aquifer underlain by Permian aquifer (K_p = 7.5 ft/d;S_p = 0.075)

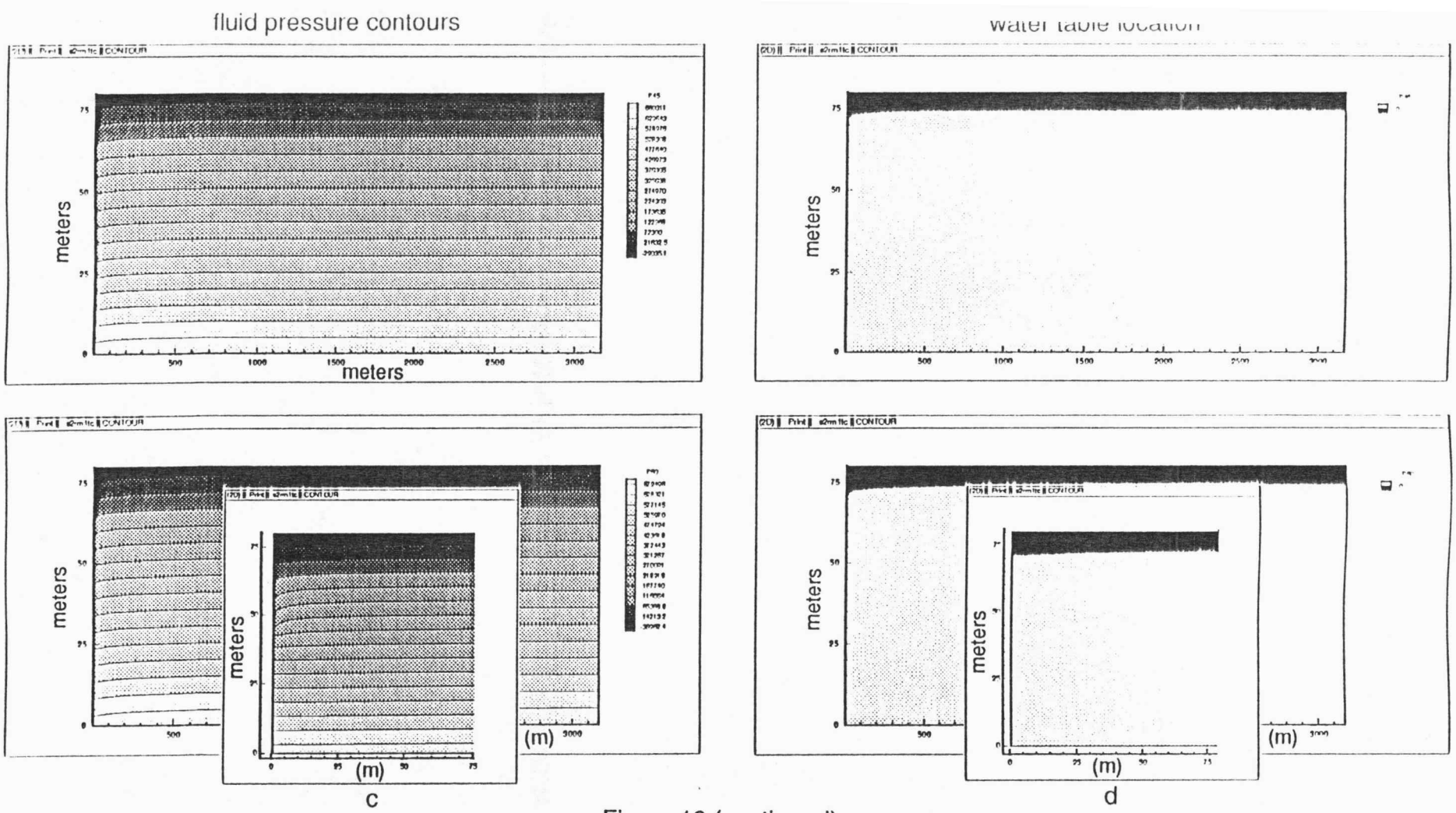

Figure 16 (continued)

Layered aquifer system: Base case alluvial aquifer underlain by Permian aquifer (K_p = 7.5 ft/d;S_p = 0.075)

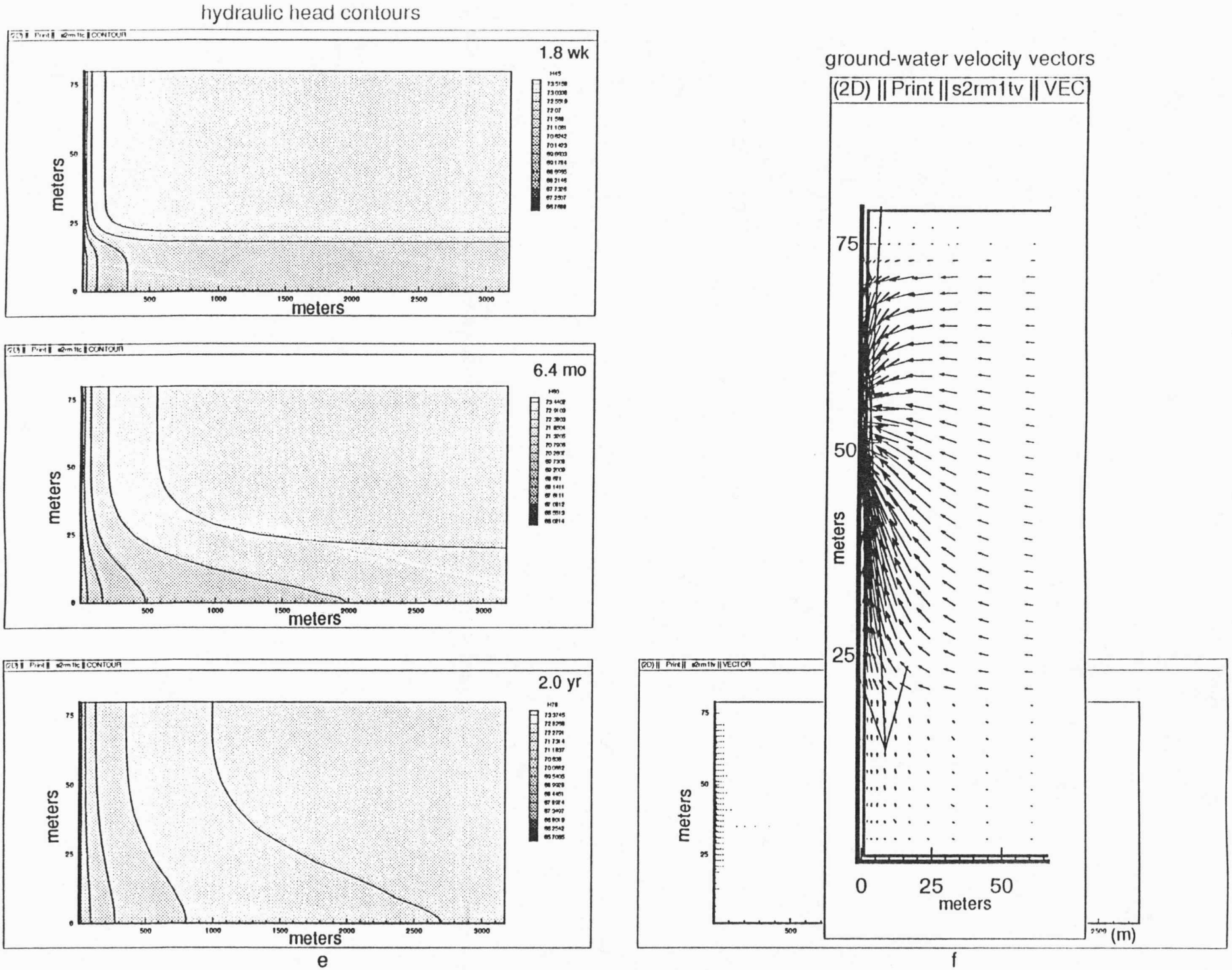

Figure 16 (continued)

Layered aquifer system: Base case alluvial aquifer underlain by Permian aquifer (K_p = 7.5 ft/d;S_p = 0.075)

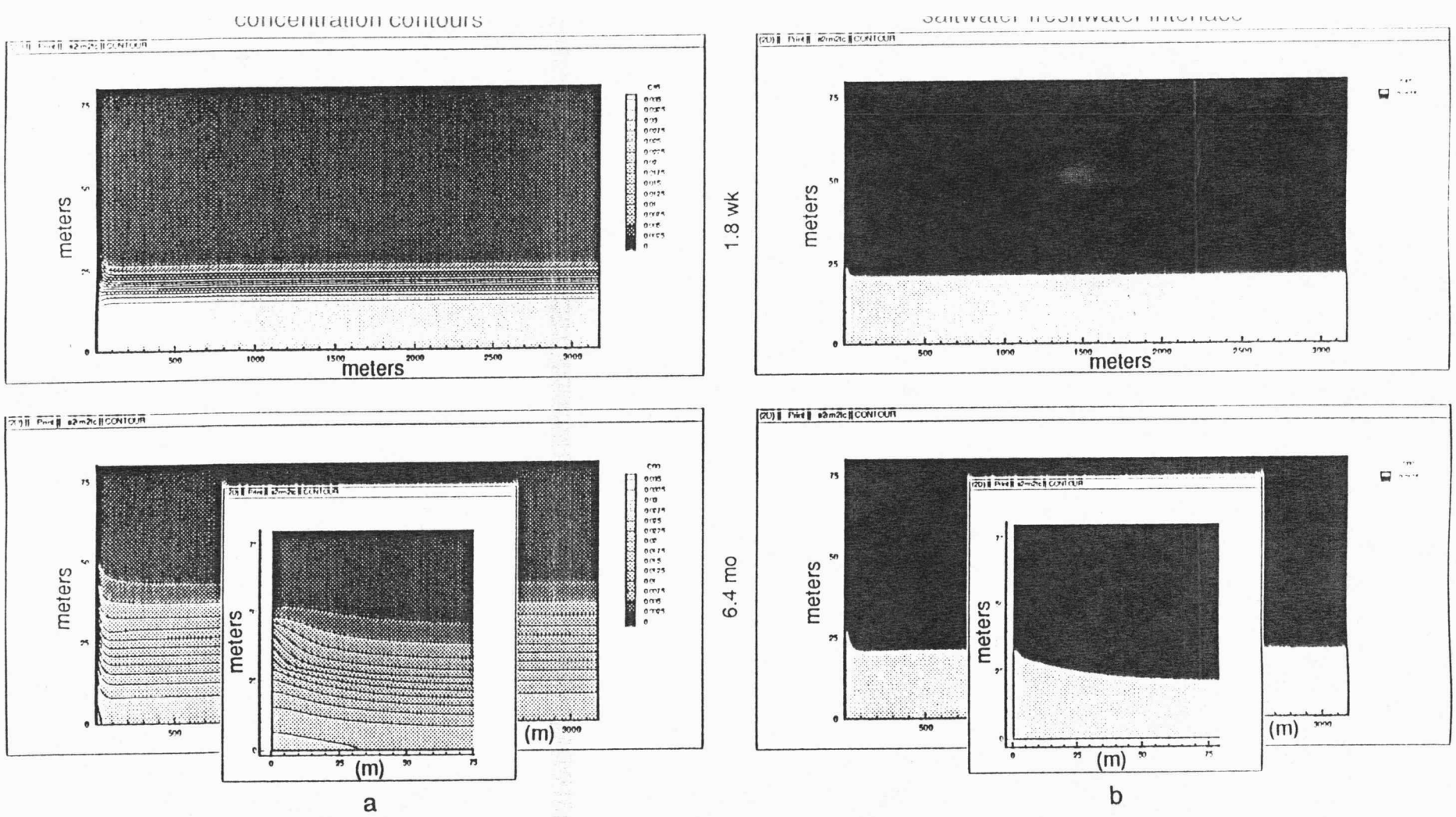

Figure 17. Case 11

Layered aquifer system but with a continuous clay layer(K_{CL}= 3.35 ft/d;S_{CL}= 0.075)

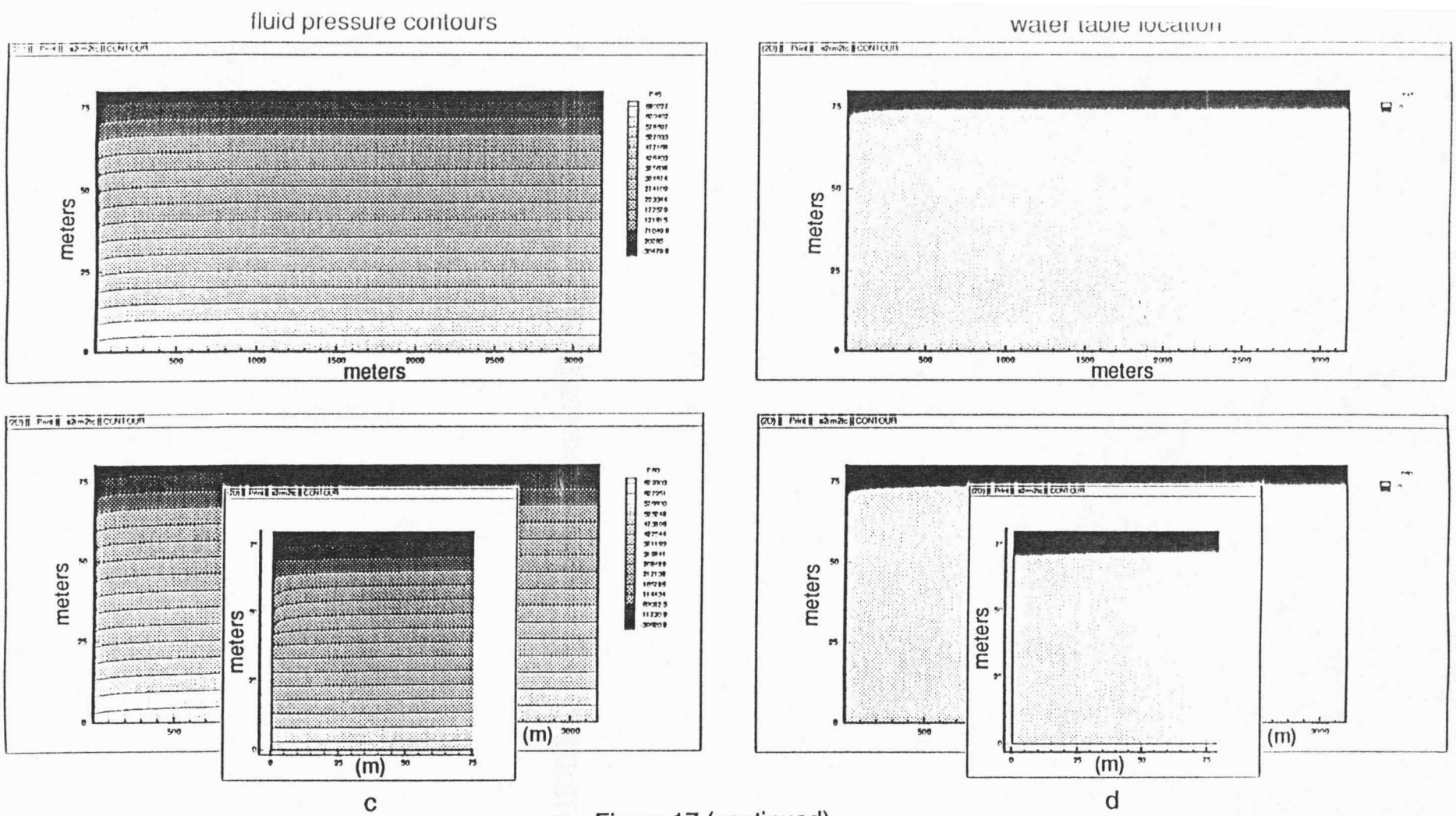

Figure 17 (continued)

Layered aquifer system but with a continuous clay layer(K_{CL}= 3.35 ft/d;S_{CL}= 0.075)

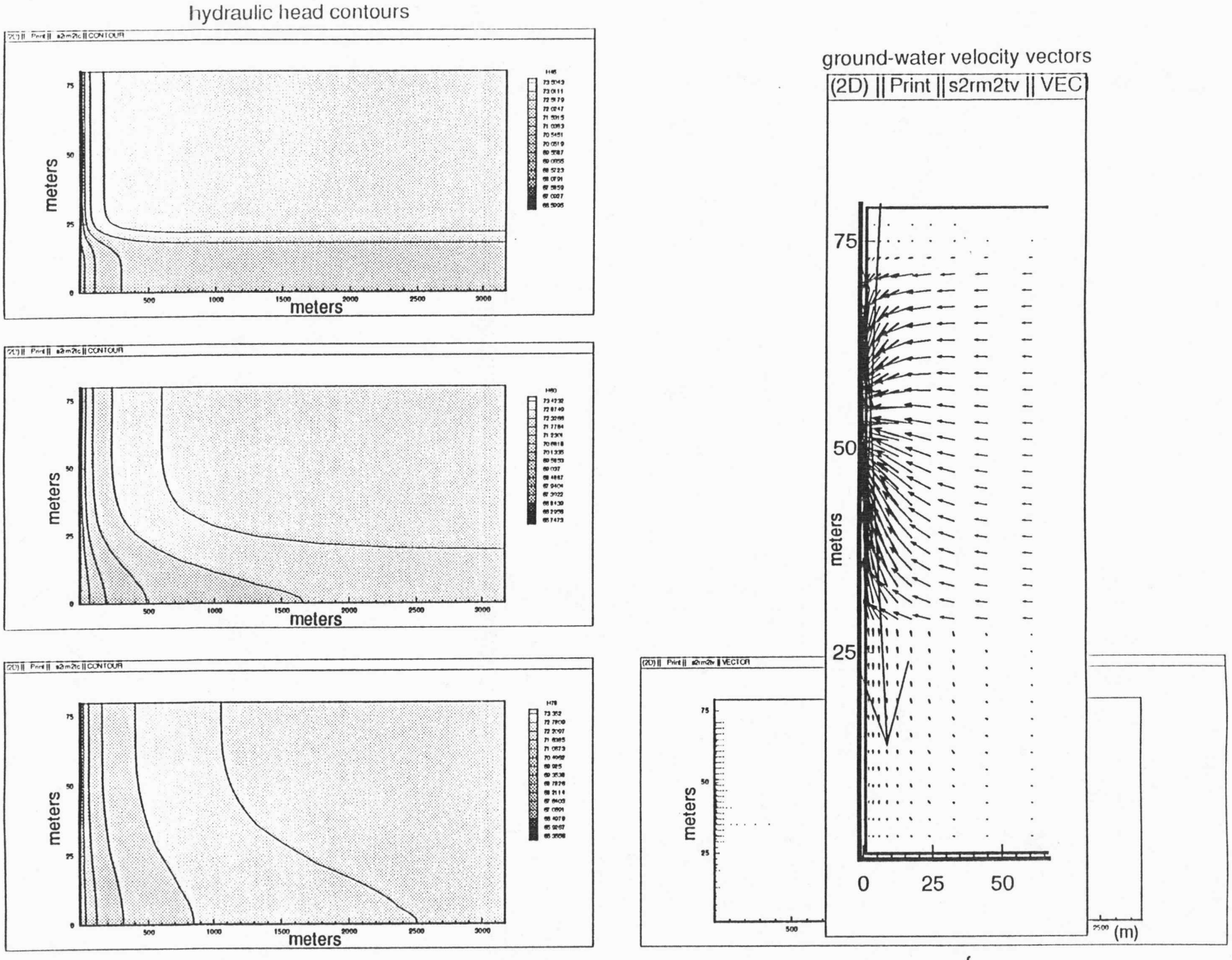

e f

Figure 17 (continued)

Layered aquifer system but with a continuous clay layer(K_{CL}= 3.35 ft/d;S_{CL}= 0.075)

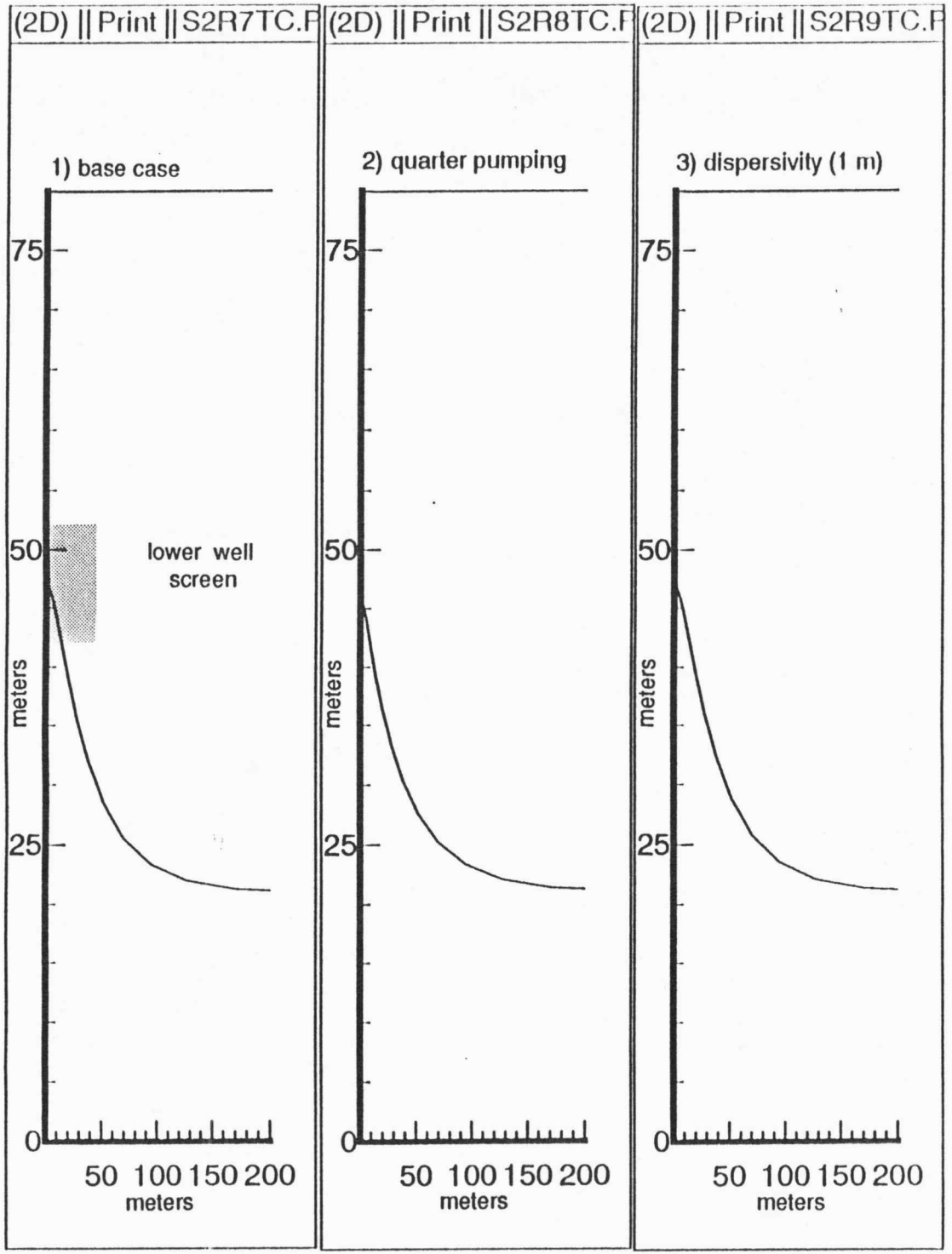
(2D) || Print || S2R7TC.P
1) base case
75
50
25
0
meters
lower well screen
50 100 150 200
meters
(2D) || Print || S2R8TC.P
2) quarter pumping
75
50
25
0
meters
50 100 150 200
meters
(2D) || Print || S2R9TC.P
3) dispersivity (1 m)
75
50
25
0
meters
50 100 150 200
meters

Figure 18

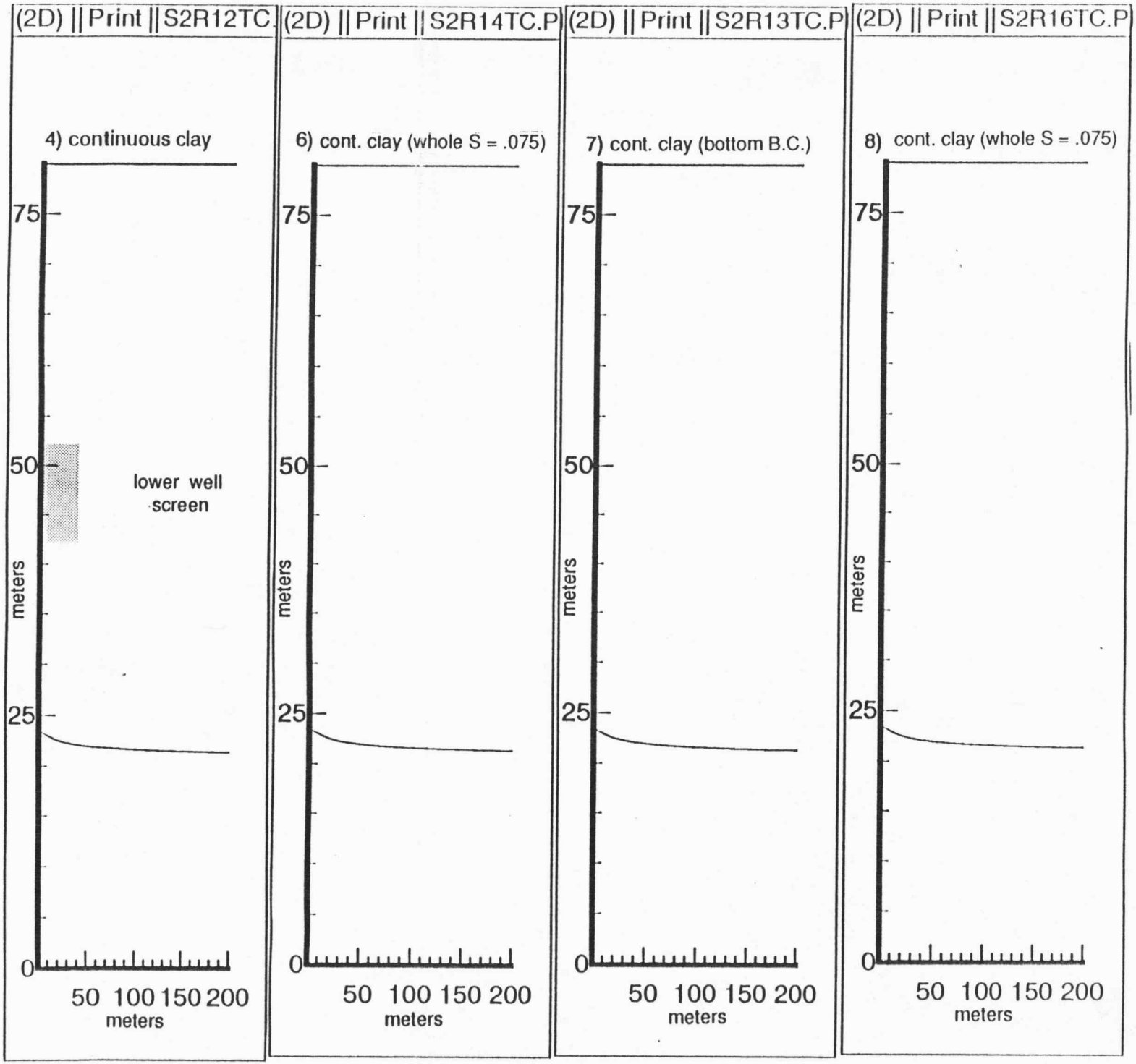
(2D) || Print || S2R12TC.
4) continuous clay
lower well screen
(2D) || Print || S2R14TC.P
6) cont. clay (whole S = .075)
(2D) || Print || S2R13TC.P
7) cont. clay (bottom B.C.)
(2D) || Print || S2R16TC.P
8) cont. clay (whole S = .075)
75
50
25
0
meters
50 100 150 200
meters

Figure 19

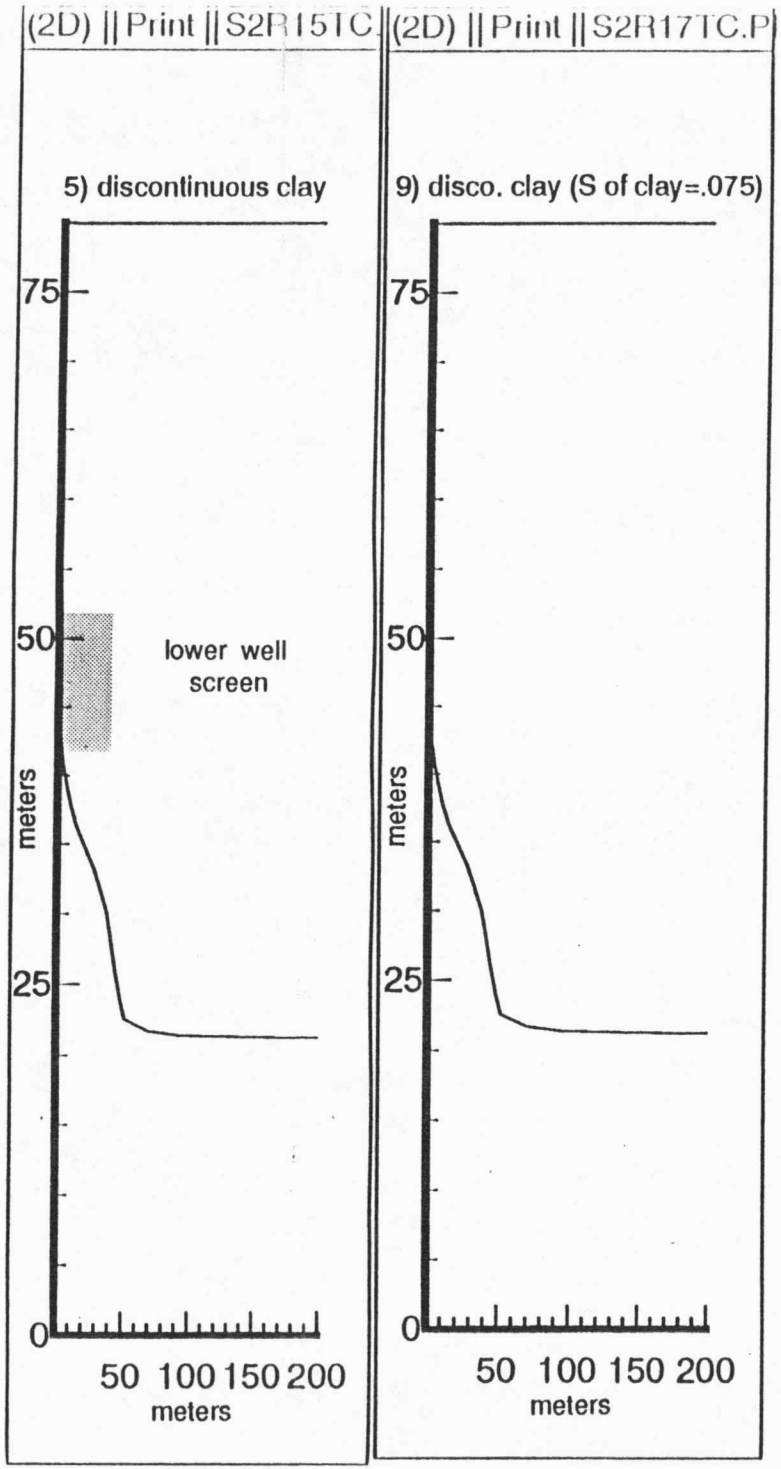
(2D) || Print || S2R15TC
5) discontinuous clay
75
50
25
0
meters
lower well
screen
50 100 150 200
meters
(2D) || Print || S2R17TC.P
9) disco. clay (S of clay=.075)
75
50
25
0
meters
50 100 150 200
meters

Figure 20

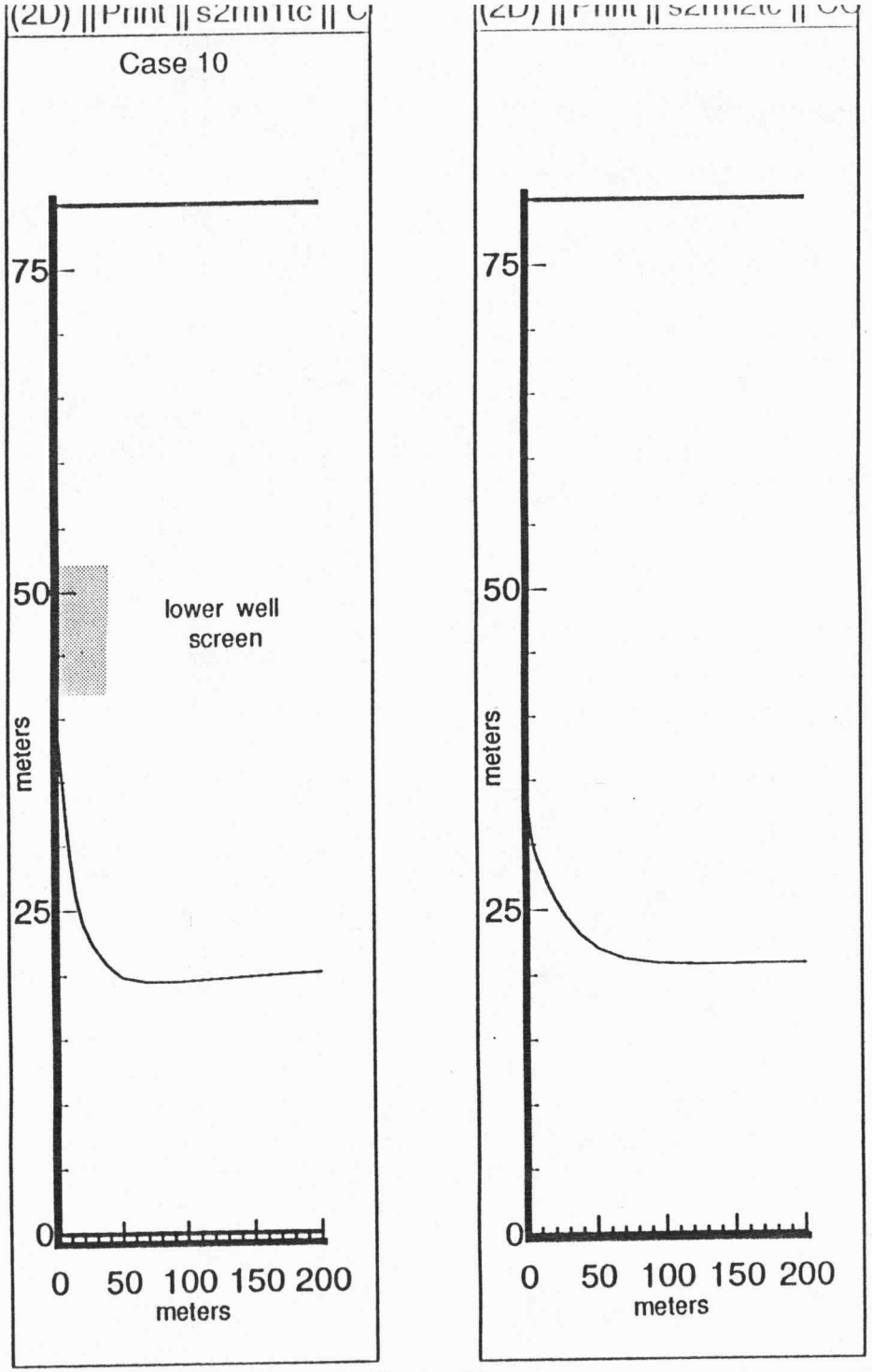
Case 10
75
50
25
0
meters
lower well
screen
0 50 100 150 200
meters
75
50
25
0
meters
0 50 100 150 200
meters

Figure 21